Title
Peculiar piezoelectricity of atomically thin planar structures

Journal
Nanoscale, 12(5)

ISSN
2040-3364

Authors
Ghasemian, Mohammad B
Daeneke, Torben
Shahrbabaki, Zahra
et al.

Publication Date
2020-02-06

DOI
10.1039/c9nr08063e

Nanoscale

ROYAL SOCIETY OF CHEMISTRY

REVIEW

View Article Online
View Journal | View Issue

Cite this: *Nanoscale*, 2020, **12**, 2875

Peculiar piezoelectricity of atomically thin planar structures

Mohammad B. Ghasemian,[a] Torben Daeneke,[b] Zahra Shahrbabaki,[c] Jiong Yang[a] and Kourosh Kalantar-Zadeh *[a]

The emergence of piezoelectricity in two-dimensional (2D) materials has represented a milestone towards employing low-dimensional structures for future technologies. 2D piezoelectric materials possess unique and unprecedented characteristics that cannot be found in other morphologies; therefore, the applications of piezoelectricity can be substantially extended. By reducing the thickness into the 2D realm, piezoelectricity might be induced in otherwise non-piezoelectric materials. The origin of the enhanced piezoelectricity in such thin planes is attributed to the loss of centrosymmetry, altered carrier concentration, and change in local polarization and can be efficiently tailored *via* surface modifications. Access to such materials is important from a fundamental research point of view, to observe the extraordinary interactions between free charge carriers, phonons and photons, and also with respect to device development, for which planar structures provide the required compatibility with the large-scale fabrication technologies of integrated circuits. The existence of piezoelectricity in 2D materials presents great opportunities for applications in various fields of electronics, optoelectronics, energy harvesting, sensors, actuators and biotechnology. Additionally, 2D flexible nanostructures with superior piezoelectric properties are distinctive candidates for integration into nano-scale electromechanical systems. Here we fundamentally review the state of the art of 2D piezoelectric materials from both experimental and theoretical aspects and report the recent achievements in the synthesis, characterization and applications of these materials.

Received 19th September 2019,
Accepted 15th January 2020

DOI: 10.1039/c9nr08063e

rsc.li/nanoscale

[a]*School of Chemical Engineering, University of New South Wales (UNSW), Sydney Campus, NSW 2052, Australia. E-mail: k.kalantar-zadeh@unsw.edu.au*
[b]*School of Engineering, RMIT University, Melbourne, VIC 3001, Australia*
[c]*School of Chemical and Biomolecular Engineering, University of Sydney, Sydney, NSW 2006, Australia*

1. Introduction

The piezoelectric effect, which was discovered in 1880 by the Curie brothers, is defined as the capability of a material to convert mechanical stimuli into electrical signals and *vice*

Mohammad B. Ghasemian

Dr Mohammad Bagher Ghasemian received a MSc degree in analytical chemistry from Iran University of Science & Technology in 2011. He holds a PhD degree in materials science and engineering from the University of New South Wales (UNSW), Australia. Currently, he is a postdoctoral research associate in the School of Chemical Engineering, UNSW, Australia, under the supervision of Prof. Kourosh Kalantar-Zadeh focusing on the preparation and application of 2D materials, liquid metals, piezoelectric materials and device fabrication.

Torben Daeneke

Dr Torben Daeneke received his PhD in chemistry from Monash University, Australia in 2012. After graduating, he held postdoctoral appointments at the CSIRO and at RMIT University (Australia). He received a RMIT Vice Chancellor's postdoctoral fellowship in 2015. In 2018 he joined RMIT's School of Engineering as a faculty member and is now a senior lecturer. His research interests span from the chemistry of liquid metals over the synthesis and functionalisation of 2D materials to materials for energy and electronic applications.

versa.[1] Generally, it is believed that piezoelectricity only appears in materials with a bandgap which also do not feature centrosymmetry in their crystal structures.[2] In metals, electrostatic forces between ions are screened by itinerant electrons. Additionally, the ferroelectric switching in metals is ruled out by screening, which excludes the external electric fields. Hence, metals do not possess piezoelectricity since polarization charges are fully screened due to the high electron concentration. However, this view has been questioned when spontaneous polarization and ferroelectricity were found in metallic WTe_2 by Fei *et al.*, suggesting a metal is also able to exhibit piezoelectricity, as if a material is ferroelectric it is piezoelectric too.[3] Deformation within piezoelectric materials, due to an external force, results in the distortion of the crystal lattice and consequently the generation of an electrical potential. Based on dimensionality, piezoelectric nanostructures are classified into four main categories of zero-dimensional (0D), one-dimensional (1D), two-dimensional (2D), and three-dimensional (3D) materials, as shown in Fig. 1.[4] The definition of 0D piezoelectricity is a new concept. Basically, it refers to nanomaterials such as nanodots, nanodispersions, heterogeneous particle arrays, uniform particle arrays, hollow spheres and core–shell quantum dots that can be assembled together in order to establish the base for other types of piezoelectric nanostructures.[5]

0D nanoparticles present high surface area, strong piezoelectric properties and intrinsic single domain; however, their practical application is limited due to assembly complications.[6] As an instance, the formation of single domains with a high piezoresponse has been observed in arrays of $PbTiO_3$ nanodots. The size dependency exploration on the piezoelectric properties of these nanodots revealed a decrease in the piezoelectric coefficient with increasing lateral size, while nanodots with diameters of approximately 10 nm preserve ferroelectricity.[7] 1D piezoelectric materials, such as nanowires, nanobelts, nanotubes and nanorods, usually have a diameter

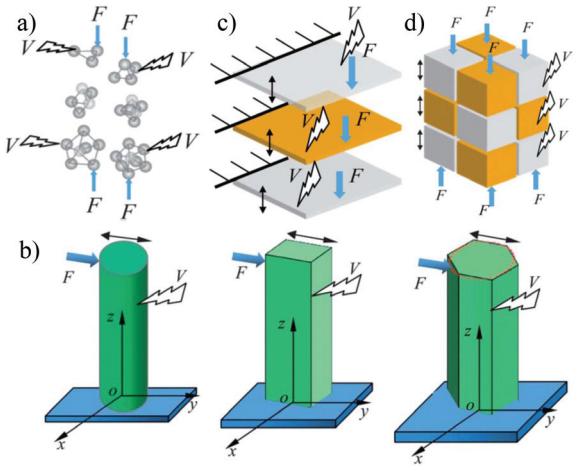

Fig. 1 (a–d) Schematic views of zero- to three-dimensional piezoelectric nanostructures. Reproduced from ref. 4 with permission from The Royal Society of Chemistry.

of less than 100 nm, which are either intrinsically piezoelectric or become piezoelectric when they lose their centrosymmetry in one or two directions.[4,8,9] 2D piezoelectric materials, which are planar structures with nanometer thicknesses, are formed from intrinsically piezoelectric materials or those which lose their centrosymmetry in one direction when thinned down. Both 1D and 2D piezoelectric nanostructures are used as building blocks of energy harvesters, catalytic systems, electronic devices and sensors.[4,10–12]

Many layered materials have been identified that feature strong in-plane bonds and weak van der Waals interlayer coupling. These layered van der Waals materials are tempting candidates for splitting off individual half unit cell thick or thicker layers through exfoliation in the search for 2D piezoelectric sheets.[13] Extensive investigations of 2D materials revealed that many of them possess unique properties, which

Zahra Shahrbabaki

Zahra Shahrbabaki is a PhD student in the School of Chemical and Biomolecular Engineering at the University of Sydney, Australia. She received a bachelor's degree in chemical engineering from the University of Tehran, Iran, in 2018. Her current research interests include the synthesis and characterization of novel materials for the assembly of electronic devices and sensors.

Jiong Yang

Dr Jiong Yang is a postdoctoral research associate under the supervision of Prof. Kourosh Kalantar-Zadeh at the University of New South Wales (UNSW) in Sydney, Australia. Before joining UNSW, he earned his PhD degree from the Australian National University. He has published over 20 highly cited peer-reviewed journal papers and book chapters on the characterization and device fabrication of two-dimensional semiconductors. His research interests include two-dimensional semiconductors, liquid metals, nano-fabrication, nano-photonics, and optoelectronic applications.

offer new opportunities to the realm of piezoelectricity, including high crystallinity paired with the exceptional ability to sustain enormous deformation/strain before failure, as well as the reduction of centrosymmetry, appearance of new electronic states and possibility of surface modifications that affect the bulk of the 2D structure.[14] In contrast to 1D and bulk piezoelectric structures, 2D piezoelectric materials can also be easily integrated with conventional surface electronic technologies, which allows the incorporation of piezoelectric devices for practical applications.[15,16]

Out of the thirty-two described 3D crystal classes, 21 crystal classes are non-centrosymmetric, while in four 2D crystal classes, including cubic, rectangular, hexagonal and oblique, the inversion symmetry can be broken by reducing the thickness from 3D to 2D of the same material composition.[17] The opportunity of inducing non-centrosymmetry when a layered crystal is thinned down, especially to monolayer thickness, offers access to a vast family of new materials for creating 2D piezoelectric structures. While some bulk materials, including many transition-metal dichalcogenides (TMDCs) and hexagonal boron nitride (h-BN), are centrosymmetric, they may reveal a broken centrosymmetry after thinning down to a single layer, due to the loss of the inversion centre. This can be achieved for materials that contain at least two van der Waals layers in their unit cell, with the inversion point being within the van der Waals gap. In contrast, monolayer graphene preserves its inversion symmetry, since the inversion centre resides within the central monolayer.[14] Altogether, the interactions between layers within stratified materials can be divided into London interactions, hydrogen bonds and interstitial cations. A wide range of compounds such as oxides, hydroxides, carbides, nitrides, halides, chalcogenides and phosphates can be prepared into a layered form,[18] and the search for 2D piezoelectric materials has so far been limited to their exfoliated form.

Raman features and phonon modes have been used for studying characteristics such as thickness, feasibility of exfoliation, stability and crystal structure of layered piezoelectric materials.[18,19] Scattering and transport of the carriers in 2D TMDCs are ruled by the material's planar structure, while the mobility of the carriers is mainly influenced by the following scattering mechanisms: (i) optical and acoustic phonon scattering, (ii) surface interface phonon scattering, (iii) Coulomb scattering at charged impurities and (iv) roughness scattering.[20,21] On the other hand, diverse factors such as carrier density, effective carrier mass, layer thickness, temperature, and phonon and electronic band structures also influence the degree that scattering mechanisms affect the mobility of carriers.[20]

Ab initio calculations have determined the phonon dispersion in WS_2 and MoS_2.[22] The obtained results correlated with the experimental Raman spectra of MoS_2 indicate that the main Raman peaks match with the out-of-plane A_{1g} mode and the in-plane E_{1u} and E^1_{2g} phonon modes. By decreasing the layer thickness of MoS_2 the position of the peaks slightly shifted due to the effect of the neighbouring layers on Coulomb interactions.[20] These peak shifts allow Raman spectroscopy to identify changes in the thickness of thin materials. Similarly, the layer thickness of atomically thin h-BN was identified relative to the intensity of the E_{2g} optical phonon mode.[23] More interestingly, the shifts in the out-of-plane and in-plane phonon coupling modes of 2D MoS_2 were employed to study its sensitivity against relative humidity.[24] By increasing the relative humidity to a certain level, the position of the A_{1g} peaks showed a blue shift due to the absorption of water molecules and change of electron–phonon interactions while the E_{2g} peaks remained unchanged. The intensity and position of Raman peaks also strongly depend on the applied strain since it changes the crystal phonons. Generally, compressive and tensile strains lead to phonon hardening (blue shift) and phonon softening (red shift), respectively. In the case of 2D materials, strain enhances the intensity of the Raman spectra which can be used for studying the properties of piezoelectric materials.[25,26] The stability of 2D Janus group-VI chalcogenides has been investigated through the molecular dynamics and phonon dispersion calculations.[27] Accordingly, MoSSe, WSeTe, WSTe, and WSSe monolayers are stable while MoSTe and MoSeTe monolayers were recognised as unstable. Also, based on the formation energy and phonon dispersion estimations, all the nine members of 2D Janus group-III chalcogenides ($GaInS_2$, $GaInSe_2$, $GaInTe_2$, Ga_2SSe, Ga_2SeTe, Ga_2STe, In_2SSe, In_2SeTe, and In_2STe) are stable.[27]

In spite of the fact that a few reviews have demonstrated piezoelectricity in two dimensions, they generally lack the depiction of important theoretical characteristics and data mining in the field of 2D piezoelectric materials. A recent review by Liu *et al.*[28] briefly demonstrated the key advances of 2D piezoelectric materials, especially in the fields of piezotronics and piezophototronics. However, the absence of theore-

Kourosh Kalantar-Zadeh

Kourosh Kalantar-Zadeh is a professor of chemical engineering at the University of New South Wales, Sydney, Australia. He is also a Laureate Fellow of the Australian Research Council. He has co-authored >425 research articles and reviews. Prof. Kalantar-Zadeh is a member of the editorial boards of several journals including Applied Materials Today, ACS Applied Nano Materials, ACS Sensors, Advanced Materials Technologies, Nano-Micro Letters *and* ACS Nano. *He is internationally recognised for his work on sensors, two-dimensional materials and liquid metals. He was a recipient of the 2017 IEEE Sensor Council Achievement and 2018 ACS Advances in Measurement Science Lectureship Awards.*

tical studies and data mining for identifying 2D piezoelectric candidates is sensed. This paper expands upon the recent progress and most important aspects of 2D piezoelectric materials from the fundamental principles to applications. We outline 2D piezoelectric materials and review the main preparation methods followed by the theoretical and experimental approaches of measuring piezoelectricity in 2D materials. Theoretical predictions of piezoelectricity and the diverse compounds discovered through data mining are presented. 2D compounds that are the topic of recent intense research and their applications are discussed.

2. Piezoelectric materials

The discovery of piezoelectricity in 2D materials[29] led to new horizons for energy harvesting systems, electronics, actuators, and sensors for employing such low-dimensional materials in the next-generation technologies. Although there are many review articles on piezoelectric materials,[10,30–34] information about the 2D piezoelectric structures is still sparse. With recent progress in the synthesis methods for materials at atomic levels, piezoelectricity in atomically thin layered materials has drawn more attention. Recent studies have evidenced many promising 2D materials for their piezoelectric properties.[2,15,26,35,36] Five important groups of 2D piezoelectric materials including h-BN, TMDCs, groups III and IV monochalcogenides and chemically modified graphene have attracted much interest in the field of piezoelectricity.[37–39] It was demonstrated that 2D TMDCs such as 2H-MoS_2, 2H-WS_2 and 2H-$MoSe_2$ present stronger piezoelectric coefficients than h-BN and engineered graphene and some of them, specifically 2H-$MoTe_2$, show remarkable piezoelectric coefficients even larger than those of 3D wurtzite materials including bulk GaN and AlN.[37,40] Based on first-principles calculations,[41] layered group III monochalcogenides including InSe, GaS and GaSe were also recognized to be piezoelectric in monolayer form. The structure of this group of monolayered materials is quite similar to that of 2H-TMDCs and both groups possess a D_{3h} point group symmetry with no inversion centre and thus nonzero piezoelectric response.

Group IV monochalcogenide 2D piezoelectrics comprising GeS, GeSe, SnS and SnSe possess a C_{2v} point group to offer colossal piezoelectricity. First principles simulations predict that monolayer group IV monochalcogenides can show strong piezoelectric coefficients approximately one to two orders of magnitude larger than those of other 2D piezoelectrics such as 2H-MoS_2 and h-BN.[42] The strong piezoelectricity in monolayer group IV monochalcogenides arises from the stable noncentrosymmetric structure of monolayers and their flexible puckered C_{2v} symmetries along the armchair direction.[43] In spite of the fact that graphene possesses many distinctive physical and mechanical properties, this 2D nanomaterial is not intrinsically piezoelectric due to its inversion symmetry factor; however, piezoelectricity can be induced in graphene through physical or chemical modifications (engineering) which will be discussed in the following sections. Although the piezoelectric polarization of 2D materials, such as h-BN and MoS_2, is usually narrowed to the in-plane orientation and odd number of layers, as an interesting group III–VI chalcogenide material, α-In_2Se_3 shows both out-of-plane and in-plane piezoelectricity proven by theoretical calculations and experimental studies.[44,45] The experimental studies assigned this in-plane/out-of-plane coexistence to the noncentrosymmetry in α-In_2Se_3 which originates from the hexagonal stacking and offers an exceptional opportunity to take advantage of both directional and nondirectional piezoelectricity in devices. According to the piezoresponse force microscopy (PFM) measurements, the d_{33} piezoelectric coefficient in α-In_2Se_3 is increased from 0.34 to 5.6 pm V^{-1} by the accumulation of layers from single to bulk without the odd/even effect and this layer dependency of in-plane and both out-of-plane piezoelectric characteristics has been associated with the substrate clamping effect in α-In_2Se_3.[44]

According to the principles of crystallography, the piezoelectric effect appears in all non-centrosymmetric point groups except for the cubic class 432. In 2D piezoelectric materials, piezoelectricity generally originates through three phenomena: (1) loss of centrosymmetry, (2) charge delocalization and (3) surface modification,[15,46] which are discussed below.

2.1. Centrosymmetry impact

Material properties and their application are significantly correlated with and impacted by their crystal symmetry. To induce the piezoelectric effect, the material needs to have a nonzero electronic band gap and a nonsymmetric crystal structure.[47,48] The lack of centrosymmetry determines the piezoelectric moduli and certain optical properties of the material. The symmetry of single or few layered materials might be different from that of their bulk counterparts, leading to new material properties that arise in 2D nanostructures. Many bulk materials lose their inversion centre when downsized to 2D, specifically to monolayer dimensions. Reduction of the dimensionality to 2D crystal structures significantly increases the anisotropy and reduces symmetry elements, which promote piezoelectricity in 2D structures such as buckled hexagonal and 2H structures with broken inversion symmetry.[37,49,50] 2H-MoS_2 and h-BN are well-known examples, which possess an inversion centre and nonpiezoelectric nature in the bulk structure, while their individual monolayers present piezoelectricity due to the lack of centrosymmetry, as shown in Fig. 2.[14,29,51] Moreover, the breaking of inversion symmetry and piezoelectricity are also observed in odd number of layers since all odd-rank tensor properties, such as the third-rank piezoelectric tensor properties, might be mathematically nonzero.[47] A computational study[48] suggested that many bulk structures with different point groups lose their centrosymmetries upon exfoliation to monolayers and statistically the percentage of structures with no centre of inversion grew from 18% in bulk crystals to 43% in monolayer counterparts for the same structure (Fig. 3a), which may potentially offer output

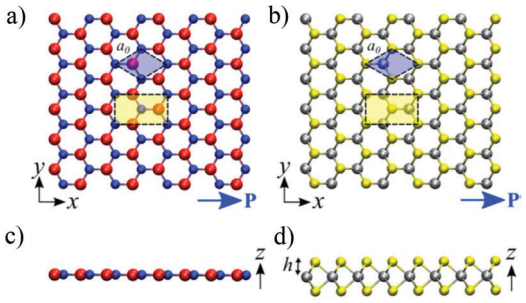

Fig. 2 (a, b) Top views and (c, d) side views of atomically thin h-BN and 2H-MoS_2, respectively. (B, N, Mo and S atoms are red, blue, silver and yellow, respectively.) The arrows show the direction of piezoelectric polarization. Hexagonal primitive cell and orthorhombic unit cell used in DFT simulations are highlighted in blue and yellow. Reprinted with permission from ref. 29. Copyright (2012) American Chemical Society.

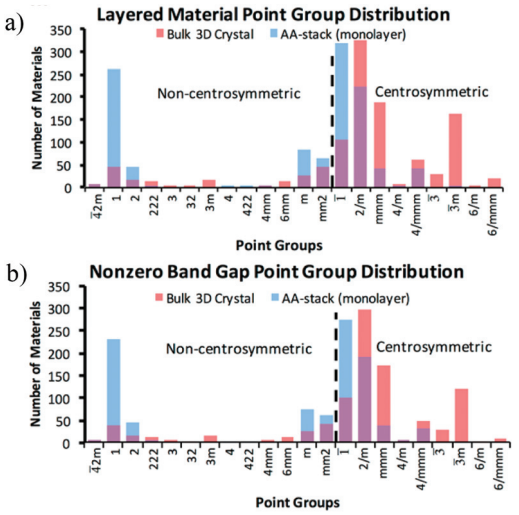

Fig. 3 Computed point groups of the identified layered materials. (a) The point group distribution of layered materials with and without centrosymmetry in the Materials Project database indicating that many bulk materials lose the centre of inversion upon exfoliation into monolayers. (b) Distribution of materials with nonzero band gaps as the essential criteria for piezoelectricity. The symmetry of primary bulk 3D crystals and their corresponding AA-stacked crystals have been shown in red and blue, respectively. Reprinted with permission from ref. 48. Copyright (2017) American Chemical Society.

power response, if possessing a nonzero electronic band gap, as depicted in Fig. 3b.

2.2. Delocalization of charges

Changes in the local polarization and lower carrier concentration are the other possible origins of creation or enhancement of piezoelectricity in materials after thinning down from the bulk to 2D nanostructures.[15] The piezoelectric effect is highly correlated with the direction of polarization, for example, the piezoelectric effect is limited in the *c*-axis of ZnO and just exists in the in-plane direction with three-fold rotation symmetry for MoS_2. ZnO nanosheets with a wurtzite structure retain their hexagonal structures even when they thinned down to a few atomic layers and thus the crystal non-centrosymmetry and piezoelectricity are preserved.[52] As shown in Fig. 4a, the centres of negative and positive ions are displaced relative to the stress applied along the apex of the tetrahedron, which motivate the piezoelectric polarization and piezoelectricity along the *c*-axis.[53] CdS is another example of a material in which piezoelectricity increases by thinning due to the delocalization of charges. CdS ultrathin films (2–3 nm) and ZnO nanosheets (2 nm) showed piezoelectric coefficients (d_{33}) of 32.8 and 23.7 pm V^{-1}, respectively, which are almost two to three times larger than those of their bulk counterparts.[53–55]

The carrier concentration (n_c) can be obtained using $n_c = 1/\rho e\mu_e$ where ρ, e and μ_e are resistivity, electronic charge and electron mobility, respectively. Previous studies implied that the piezoelectricity in materials significantly depends on the carrier concentration.[56] For example, CdS thin films synthesized by chemical vapor deposition exhibited a carrier concentration of $\sim 10^{12}$–10^{15} cm^{-3}.[54] By increasing the carrier concentration from 10^9 to 10^{18} cm^{-3} in CdS, the piezoelectric coefficient dropped by 60%.[57,58] It was suggested that the stronger piezoelectricity in CdS ultrathin films arises from a lower carrier concentration, free boundary and change in local polarization due to the small dimensionalities with a large surface area, and charge and defect redistribution near the surfaces.[53,54,59]

2.3. Surface modification

Piezoelectricity in 2D materials can originate from surface and structural modifications. A non-centrosymmetric structure and subsequently piezoelectric characteristics can be produced in 2D materials through appropriate crystal engineering and material modification. The most widely studied monolayer material, graphene,[60,61] typically possesses an inversion symmetry and is not naturally piezoelectric. However, single-layer graphene deposited on SiO_2 grating substrates presented a considerable vertical piezoelectric coefficient of 1.4 nm V^{-1}. As shown in Fig. 4b, this piezo-response was associated with the broken symmetry of the crystal structure due to the chemical interaction of carbon atoms in graphene with the oxygen atoms of the underlying SiO_2 substrate. This chemical interaction induces a non-zero dipole moment and polarization in the system.[62] Similarly, there are other examples of generating piezoelectricity in 2D graphene by selective chemical modification or introducing structural defects.[39,63–65] The flexoelectricity concept has been introduced to rationalize the emerging piezoelectricity in porous graphene sheets having holes with defined symmetries and shapes. The average strain gradient around the hole is non-zero due to the broken inversion symmetry; therefore, flexoelectricity causes local polarization and generally a non-zero net polarization in the graphene sheet, as described in Fig. 4c and d.[66] Theoretical[67–70] and experimental[71–73] studies have proven that piezoelectricity can be engineered into graphene through the selective adsorption of adatoms on the surface. Calculations carried out by Ong *et al.* showed that employing H, Li, K and F on single-layer graphene could result in the change of polarization (Fig. 4e) and

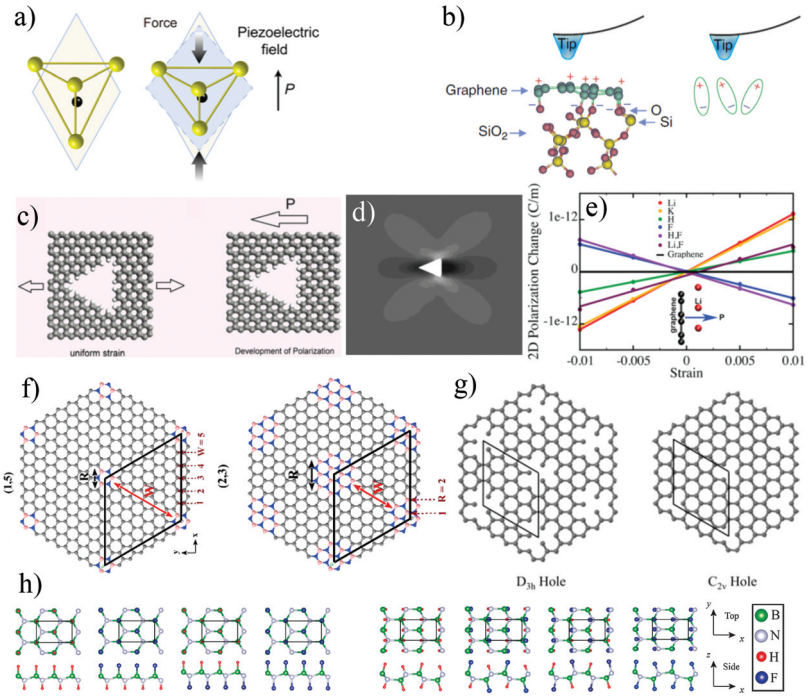

Fig. 4 (a) Hexagonal structure of the ZnO nanomaterial with Zn–O–Zn stacking while the O atom is in the centre of the tetrahedron before compression (left) while a piezoelectric field is generated when the unit cell of ZnO is compressed by an external force (right). Reprinted with permission from ref. 53. Copyright (2018) American Chemical Society. (b) Schematic of a graphene layer with oxygen termination on a SiO_2 substrate (left) and generation of oriented dipolar surface states adjacent to the substrate surface as the origin of the piezoresponse due to the chemical interaction between carbon and oxygen atoms (right). Reproduced from ref. 62. CC BY 4.0. (c) The emergence of polarization in a triangular-hole graphene nanosheet under the applied strain and (d) a finite element model showing the qualitative nature of distribution of strain towards the triangular hole in a thin sheet based on the linearized elasticity theory. Reprinted from ref. 66, with the permission of AIP Publishing. (e) Presence of piezoelectricity in an engineered graphene single sheet doped with different atoms on the surface due to broken inversion symmetry. Polarization changes perpendicular to the graphene sheet by applying an equibiaxial in-plane strain to graphene which can be used for determining the e_{31} piezocoefficient. The inset indicates the direction of positive polarization. Reprinted with permission from ref. 39. Copyright (2011) American Chemical Society. (f) Different configurations of piezoelectric graphene doped with BN. R and W are the radius of BN rings and the width of the separating wall, respectively, and the enclosed areas show the unit cell of each configuration. (g) D_{3h} and C_{2v} point symmetry defects (holes) in graphene which break the inversion symmetry of graphene. Unit cells are enclosed with black lines. Reprinted with permission from ref. 63. Copyright (2015) American Chemical Society. (h) Top and side views of surface-modified h-BN with hydrogen and/or fluorine atoms; the left and right groups are chair and boat forms respectively, and the unit cells are shown with rectangles. Reproduced from ref. 74 with permission from the PCCP Owner Societies.

the generation of piezoelectricity in graphene by breaking the inversion symmetry, leading to piezoelectric coefficients that are comparable with those of 3D piezoelectric materials such as wurtzite BN and GaN, as listed in Table 1. The highest d_{31} piezoelectric coefficient in graphene was obtained after modification with F and Li whereas doping with Li or K resulted in the highest e_{31} piezoelectric coefficient.[39,60] 2D graphene also becomes piezoelectric by substituting its carbon pairs with different patterns of BN, which transforms the point symmetry of graphene from D_{6h} (centrosymmetric) to D_{3h} (non-centrosymmetric). Similarly, hole defects may induce D_{3h} or C_{2v} point symmetries, which break the inversion symmetry in graphene, as shown in Fig. 4f and g.[63] Although h-BN monolayers are intrinsically piezoelectric, chemical doping such as fluorination and hydrogenation may be applied on both sides of h-BN to induce flatness distortion and consequently produce new in-plane and out-of-plane dipole moments and piezoelectric responses in h-BN (Fig. 4h).[74]

Table 1 Piezoelectric coefficients (d_{31} in pm V^{-1} and e_{31} in pC m^{-1}) in graphene after chemical doping with K, Li, H, and F adatoms calculated by density functional theory (DFT). Bulk wurtzite BN[76] and GaN[77] are listed for comparison. Reprinted with permission from ref. 39. Copyright (2012) American Chemical Society

Atom(s)	d_{31}	e_{31}
K	0.23	52
Li	0.15	55
H	0.11	20
F	0.0018	−26
F, Li	0.30	30
H, F	0.034	−31
3D BN	0.33	—
3D GaN	1.05	—

2.4. Piezoelectric polarization direction

Polarization is a crucial concept in piezoelectric materials for understanding their response to the externally applied stimuli.

By the application of an electric field, dipoles are created by changing the position of electrons and nuclei and consequently the material undergoes polarization. In addition to the electric field, polarization occurs in piezoelectric materials by the application of a mechanical stress. Negative and positive charges neutralize each other; therefore, piezoelectric materials do not show any current flow under zero-load conditions. However, by applying compacting or stretching forces, a voltage appears due to the imbalance of the dipole moments.[75] The selection of piezoelectric materials for particular applications requires a standard mean to identify the direction of polarization and set the electrical and mechanical axes of operation. These axes are described by numbers, for instance, 1, 2 and 3 corresponding to the x, y and z axes, respectively, which are set during the poling process.[75,78] The polarization direction aligns with the direction of the applied electric field through the poling process when the material is subjected to a sufficiently large electric field. The poled materials retain the polarization direction even after the external field is ceased and exhibit piezoelectric properties.[79] Applying a mechanical tension or compression on a poled piezoelectric material alters the dipole moments and generates voltage. The direction of the poling field leads the direction of the electrical and mechanical axes. When a compression happens along the polarization direction or a tension happens perpendicular to the polarization direction, a voltage with the same polarity of the poling voltage is generated. On the other hand, compressions perpendicular to or tensions along the polarization direction lead to a voltage with opposite polarity to that of the poling voltage. These behaviours are known as generator actions.[80]

The direction of piezoelectric polarization is sequentially switched by changing the orientation of the applied strain tensor. Therefore, the mechanical and electrical behaviours of piezoelectric materials can be coupled through the $S_{ij} = d_{kij}E_k$ equation where s, d and E represent the second rank strain tensor, piezoelectric coefficient and electric field, respectively (i, j and k stand for x, y and z of the Cartesian frame).[81] Piezoelectricity in 2D materials is highly correlated with the direction of polarization, which can be in-plane, out-of-plane or both and can potentially play an important role in the development of future planar devices if harnessed correctly and efficiently. While many 2D materials show in-plane intrinsic piezoelectricity, out-of-plane ferroelectricity and piezoelectricity are more straightforward and applicable for circuit designs such as nanogenerators, nonvolatile memory and photovoltaic devices.[82]

TMDCs, h-BN and graphene nitride possess in-plane piezoelectricity. As an example of TMDC materials, the piezoelectric property of MoS_2 is only restricted to the in-plane (d_{11}) direction and no out-of-plane (d_{33}) direction is found since MoS_2 monolayers preserve the ideal symmetry feature along the vertical z-axis, as shown in Fig. 2b and d.[51] Also, due to the unique hexagonal structure, the in-plane piezoelectric field vector in 2D MoS_2 has three equal directions, which are along the three-fold symmetry axes.

In contrast to graphene, h-BN shows intrinsic piezoelectricity with a strong in-plane direction due to the alternating sequence of nitride and boron atoms in the hexagonal array.[36] Although the noncentrosymmetrical structure and the lack of an inversion centre are known as the basic origins of intrinsic piezoelectricity, extrinsic piezoelectricity and polarized dipoles can be induced in 2D materials by applying special interfaces, *e.g.* doped graphene with out-of-plane piezoelectricity, which will be discussed in the following section.

Some materials such as rhombohedral α-In_2Se_3 and Janus MoSSe exhibit more intricate piezoelectricity in both in-plane and out-of-plane directions.[82–84] In the synthesis of 2D Janus MoSSe through plasma stripping and thermal selenisation, one layer of S atoms in MoS_2 can be artificially replaced by a layer of Se atoms, which creates a broken out-of-plane symmetry and vertical piezoelectricity in 2D MoSSe, which are not observed in pristine 2D MoS_2. Besides that, such a Janus MoSSe monolayer takes advantage of the in-plane piezoelectric effect due to atomic planar projections similar to those of the TMDC family.[84]

3. Preparation techniques of 2D piezoelectric materials

To date, many synthesis methods have been developed for the preparation of 2D materials which mainly can be divided into two main groups of "top-down" and "bottom-up" methods. In the first approach, bulk hosts of layered materials are delaminated into their elemental layers, while materials are grown "atom by atom" under special conditions in the latter method.[85] Although various synthesis approaches have been developed,[43] two major methods of exfoliation from the bulk and direct growth by vapor phase deposition are the dominant methods. In this section, different synthesis methods for the synthesis of 2D materials are discussed with the emphasis on those materials with piezoelectric properties.

3.1. Exfoliation

Generally, exfoliation is the process of dividing bulk layered materials into their mono- or few-layered flakes by overcoming the van der Waals interactions between the adjacent layers.[86,87] Bulk layered materials are defined as compounds with periodic layered structures held together by weak interlayer noncovalent attractions and strong intralayer covalent bonds.[18] Exfoliation techniques have developed considerably[88,89] and new exfoliation derivative methods such as mechanical cleavage,[13] ion intercalation[90] and surfactant-assisted ultrasonication[91] were further developed. During mechanical exfoliation, the interlayer potential energies are reduced by applying an external mechanical force. Mechanical exfoliation techniques gave birth to graphene and the technique was later extended to other related 2D materials such as phosphorene, h-BN, TMDCs and MXenes.[13,86,88,92–94]

2D materials obtained through mechanical exfoliation are of remarkably high quality with clean surfaces and high crys-

tallinity, and as a result are considered to possess superior physical properties including those which are important for piezoelectricity. However, the large-scale production of 2D materials *via* exfoliation techniques is limited because of the associated low production rate and small yields of this technique, which might possibly be improved by liquid exfoliation. In this regard, ultrasonic wave agitation has been extensively used for generating cavitation bubbles and breaking up layered crystals, allowing the production of exfoliated nanosheets.[18,88] However, such liquid phase techniques interfere with crystallinity and sheet size and will induce surface adsorbents to the final 2D sheets which can severely impact their piezo properties.

As another exfoliation approach, the chemical exfoliation method including solvent-assisted exfoliation or liquid phase exfoliation (LPE)[13,92] and ion intercalation assisted exfoliation have been used for the large-scale preparation of 2D materials. Layered compounds such as BN, Bi_2Te_3, C_3N_4, MoS_2, $MoSe_2$, $MoTe_2$, $NbSe_2$, $NiTe_2$, $TaSe_2$, and WS_2 were exfoliated by direct sonication in organic solvents (like isopropanol and *N*-methylpyrrolidone) and deposited on a large scale or as individual flakes and nanosheets.[64,92,95] Inevitably, LPE introduces functional groups and/or reduces the stoichiometry of the as-prepared 2D materials altering the chemical composition from that of the bulk, which might adversely affect their properties.[86] Specifically for 2D TMDCs, the intense and invasive LPE methods transform the crystal structure from the dominant 2H structure that does not feature centrosymmetry into semi-metallic 1T polymorphs which feature weak piezoelectricity and high electrical conductivity.

The exfoliation energies of many parent bulk materials were estimated through high-throughput screening of material databases to identify probable candidates for exfoliation to 2D materials.[18,96] In the process of producing 2D materials, the values of two closely related factors of binding energy between layers (E_B) and exfoliation energy (E_{XF}), the required energy for removing an individual layer, are extremely important. Björkman *et al.*[97] estimated the interlayer binding and exfoliation energies in a large number of layered materials by different methods. Calculations showed that the difference between E_B and E_{XF} is small and less than 4%; thus interlayer binding energy can be assumed to be equal to the exfoliation energy in all layered materials. Moreover, computational results indicated that these energies for most systems, independent of their electronic structure, are between 13–21 meV $Å^{-2}$, as shown in Fig. 5a–e.[97] A topology-scaling algorithm search in the Materials Project crystal structure database by Ashton *et al.* nominated 826 stable layered materials that can be exfoliated to 2D monolayers, while most of them (680) showed an exfoliation energy lower than 150 meV per atom, the threshold of exfoliation energies for experimentally existent materials, as demonstrated in Fig. 5f.[98] Similarly, a high-throughput computational study determined 1825 candidates for exfoliation with 1036 easily exfoliable and 789 potentially exfoliable layered materials.[99]

3.2. Chemical vapour deposition

Atomically thin films or flakes can be prepared directly on specific substrates by depositing the desired compounds from their gaseous phase or through reactions of gaseous precursors in the vapor phase, leading to deposition methods which offer 2D highly controllable layers that can achieve large area coverage with good uniformity and high crystallinity. Such layers can be of suitable physical quality to offer the predicted piezoelectricity of specific 2D systems. Additionally, the direct formation of 2D layers on a substrate that features different crystalline and chemical properties from the deposited compound can provide an inherent non-symmetry that can boost the piezoelectric coupling coefficients. Chemical vapor deposition (CVD), as one of the main approaches of vapor phase

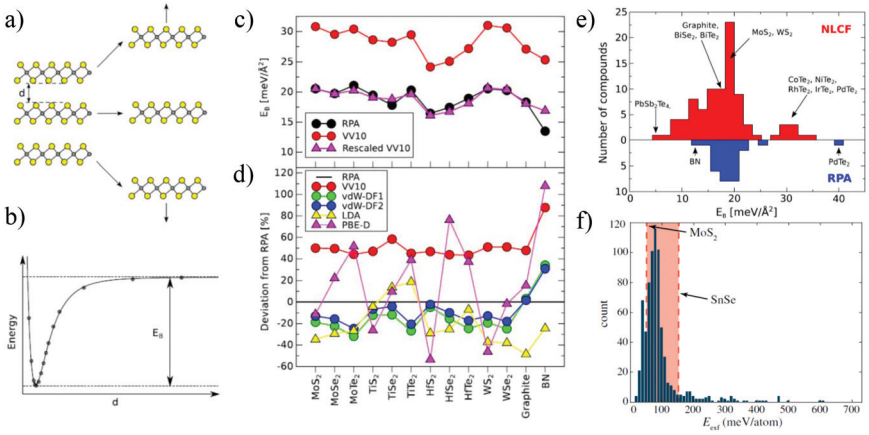

Fig. 5 (a) The process of increasing the interlayer distance for calculating the interlayer binding energy and (b) the corresponding binding energy curve. (c) Interlayer binding energies for a series of materials calculated by random-phase approximation (RPA) and the Vydrov and van Voorhis (VV10) methods. (d) Comparison of the results of different DFT-based approaches for treating van der Waals (vdW) interactions to assess their relative deviations from RPA. Reprinted figure from ref. 97. Copyright (2012) by the American Physical Society. (f) The exfoliation energy histogram calculated by DFT for 826 layered materials and (e) their comparison with experimentally synthesised 2D MoS_2 and SnSe. Reprinted figure from ref. 98. Copyright (2017) by the American Physical Society.

deposition, introduces thin layers of materials by the chemical reaction of volatile precursors on substrates.[100] Due to controllable adjustment of the thickness and acceptable electronic properties, different types of 2D piezoelectric materials such as In_2Se_3, MoS_2, $MoSe_2$, WS_2, and WSe_2 [101–105] have been synthesized using the CVD technique. CVD is frequently considered to be the most practical approach for synthesizing TMDC monolayers. Early reports on the synthesis of MoS_2 were based on the growth of multilayer materials from S and MoO_3 precursors[106,107] or through the sulfurization of a Mo-deposited substrate.[108]

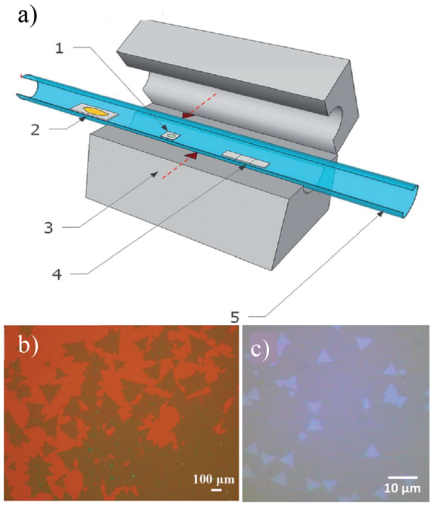

Fig. 6 (a) The schematic of chemical vapour deposition of MoS_2. 1 to 5 legends in order are: MoO_3 nanopowder, sulfur powder, horizontal furnace, quartz substrates for deposition and quartz tube. Reproduced from ref. 107 with permission from The Royal Society of Chemistry. Optical images of CVD-grown (b) MoS_2 (reproduced from ref. 109. CC BY 4.0) and (c) $MoSe_2$ (reprinted with permission from ref. 103. Copyright (2014) American Chemical Society).

Fig. 6 schematically describes the CVD principles of synthesizing 2H-MoS_2 by the chemical reaction of MoO_3 and S on the Si/SiO_2 substrate at elevated temperature.

The technique may also produce 2H-$MoSe_2$ when using the Se precursor.[103,110] In addition to the mentioned advantages of CVD over exfoliation methods, such as large-scale preparation and well-dispersed monolayers on the substrate, CVD also provides a route to directly grow layered heterostructures with clean interfaces, which are attractive for piezotronic device applications.

3.3. Liquid metal-based printing

Many 2D materials including Ga_2S_3,[111] GaS, In_2S_3,[112] SnO,[113] and γ-AlOOH[114] that are not accessible with existing synthesis methods can be feasibly prepared through the liquid metal-based reaction route using low melting point metals such as gallium and its eutectic alloys.[115] Recently, Zavabeti *et al.*[116] developed a unique technique to synthesis large area ultrathin 2D metal oxides using nontoxic eutectic gallium-based liquid alloys as a reaction environment at room temperature to isolate metal oxide nanosheets, including Al_2O_3, HfO_2 and Gd_2O_3, from the liquid metal surface through two synthesis approaches. The first is a van der Waals (vdW) exfoliation technique[117] in which the liquid metal droplet is touched by a solid substrate, where the oxide skin is isolated due to the absence of macroscopic forces between the oxide skin and the parent liquid metal (Fig. 7a and b). In the second method, pressurized air passes through the liquid metal placed under deionized water, as shown in Fig. 7c. The oxide nanosheets that formed due to the reaction between the injected air and the liquid metal are dispersed into the aqueous solution as the air bubbles are released. 2D piezoelectric $GaPO_4$ which is not achievable by conventional exfoliation was also synthesized by a liquid metal-based printing process followed by a secondary vapor phase reaction.[118] Ga_2O_3 nanosheets were first exfoliated directly from liquid gallium onto a substrate (SiO_2/Si wafer)

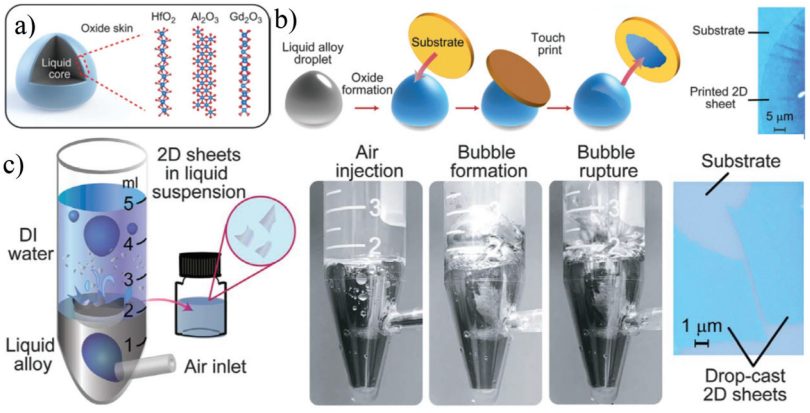

Fig. 7 (a) Thin layers of Al_2O_3, Gd_2O_3 and HfO_2 shown on the cross-section of the liquid metal. (b) vdW exfoliation technique through the touch print of a solid substrate on the surface of the liquid metal which allows the transfer of interfacial oxide layer to the substrate. (c) Schematic description of the pressurized gas injection method into the liquid metal and bursting of the formed bubbles into the upper solution. A drop-cast resulting sheet has been imaged on a SiO_2/Si wafer (right). Adjusted with permission from ref. 116. Copyright 2017 American Association for the Advancement of Science.

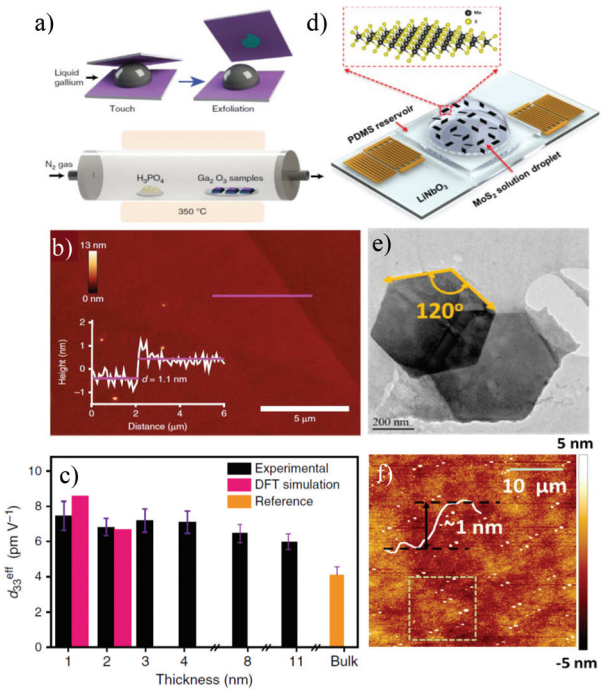

Fig. 8 (a) The exfoliation of a Ga_2O_3 nanosheet by the vdW 2D printing method from the surface of a gallium liquid metal followed by a phosphatisation step through the chemical vapour phase reaction to produce $GaPO_4$. (b) AFM topography and height profile of the aforementioned $GaPO_4$. (c) d_{33} values of $GaPO_4$ films with different thicknesses obtained through PFM measurements and DFT simulations. Reproduced from ref. 118. CC BY 4.0. (d) The MoS_2 monolayer produced in the liquid phase using an asymmetric microcentrifugation surface acoustic wave device comprising $LiNbO_3$ chips connected to the PDMS reservoir. Reprinted with permission from ref. 126. Copyright (2018) American Chemical Society. (e) Low-resolution bright-field TEM image of two stacking InSe nanosheets directly grown by pulsed laser deposition (PLD) and (f) AFM image of the triangular InSe monolayer inside the square. Reprinted with permission from ref. 120. Copyright (2017) American Chemical Society.

and subsequently phosphatized during a chemical vapor reaction in a tube furnace with phosphoric acid to result in $GaPO_4$ with a thickness of 1.1 nm, as shown in Fig. 8a–c. Employing PFM measurements and density functional theory simulation, significant experimental and theoretical vertical piezoelectric coefficients of 7.5 and 8.5 pm V^{-1}, respectively, were observed for these unit cell thick $GaPO_4$ nanosheets.

3.4. Other methods

There are also other types of deposition methods based on molecular beam epitaxy and physical deposition techniques that can result in high quality 2D crystals that should be tested for creating piezoelectric materials. Hydrothermal methods and salt-assisted and graphene-assisted synthesis techniques are further possibilities for the preparation of 2D materials that can be potentially used for making 2D piezoelectric layers.[27,85]

High quality $MoSe_2$ thin films were successfully grown layer-by-layer from monolayer to eight layers by molecular beam epitaxy (MBE) and *in situ* angle-resolved photoemission spectroscopy (ARPES) was used to study the transition from indirect to direct bandgap in $MoSe_2$ thin films with variable thickness.[119] Pulsed laser deposition (PLD) is classified as a typical physical bottom-up approach for the deposition of complicated oxide thin films;[120] however, this technique has been recently used for growing 2D materials owing to the precise control of thickness and stoichiometry, which are potential piezoelectric candidates.[121] Yang *et al.*[120] reported the direct growth wafer-scale synthesis of single phase 2D InSe nanosheets by PLD with a nominal thickness of ~1 nm (Fig. 8e and f). The PLD technique has also been used for the preparation of 2D 2H-MoS_2 [122–124] and Yb/Er co-doped WSe_2.[125] An interesting consideration is that the piezoelectricity of layered structures can assist in their exfoliation. Besides the conventional exfoliation methods, piezoelectric MoS_2 monolayers were obtained using a compact microcentrifugation surface acoustic wave (SAW) device which applied a concomitant mechanical shear force and electric field for the efficient exfoliation of layered bulk materials, shown in Fig. 8d.[126]

This developed SAW system presented a remarkable yield per unit time of 3.816% h^{-1} which is significantly higher than those of other liquid phase exfoliation methods such as probe sonication with an aqueous surfactant (0.625% h^{-1})[95] and liquid exfoliation using a blender with an aqueous surfactant (0.40% h^{-1}).[127] Nebulization using SAW devices can also result in high efficiency and ultrafast exfoliation of MoS_2.[128]

4. Characterization of piezoelectricity in 2D materials

By thinning down to the nanoscale, many macroscopic methods are not suitable for the characterization of 2D piezoelectric materials. To date, different approaches have been introduced and developed in both theoretical and experimental areas to study 2D piezoelectric materials. Although each method might be used for understanding a particular aspect of the material, a variety of characterization techniques and their combination are usually employed to ascertain the comprehensive characterization of piezoelectricity in 2D nanomaterials. Density functional theory (DFT), molecular dynamics simulations (MD) and molecular structural mechanics (MSM) can be highlighted as the most commonly used atomistic simulation methods of determining piezoelectricity in 2D materials; meanwhile, experimental techniques such as piezoresponse force microscopy (PFM) and direct tensile testing are employed to confirm these properties in parallel with theoretical studies.[43] The following section presents a brief review of the simulation and experimental approaches for investigating the piezoelectric properties of 2D materials.

4.1. Theoretical assessments

In parallel with the experimental explorations of new 2D piezoelectric materials, theoretical and simulation research on the

piezoelectric characteristics of 2D nanostructures has also emerged, to complement experimental studies on 2D piezoelectric materials.[2,49,129–132] Today, many reviews on different types of bulk piezoelectric materials can be found,[1,4,8,10,133,134] while experimental studies on 2D piezoelectric materials are limited to a few well-known 2D nanostructures (*e.g.* h-BN and MoS_2)[35,89,135–139] and systematic data collection in monolayer symmetries for probing piezoelectricity in 2D materials has been rarely reported. Theoretical calculations and simulations can now predict piezoelectricity in novel 2D materials that has never been demonstrated through experiments. As a result, the gap of knowledge in the domain of 2D piezoelectricity appears to be filling fast through data mining of 2D materials in recent reports. Data mining promotes the fast scanning of all materials in a database to identify many unexplored materials which are often not just confined to the well-studied material families that would have been otherwise unlikely to be recognized through experimental techniques. Recently, several groups of 2D materials such as piezoelectric monolayers, electrode materials and heterostructures have been established on the basis of high-throughput computations and data-mining algorithms.[18]

Ashton *et al.*[98] carried out a data mining investigation of the Materials Project crystal structure database using a topology-scaling algorithm (TSA) to recognize materials with potential layered motifs in their crystal structures through measuring the sizes of bonded atomic clusters in different unit cells (Fig. 9a). Their search yielded 826 promising layered materials as potential candidates for the production of 2D monolayer structures after exfoliation. The calculated data indicated that some stable planes such as buckled structures, as shown in Fig. 9b, could possess piezoelectricity due to their broken inversion symmetry.

Cheon *et al.*[48] carried out an intensive data mining survey on around 50 000 inorganic crystals and discovered hundreds of unrecognized low-dimensional layered structures including 325 potential 2D piezoelectric materials. A data mining algorithm was employed to find lattice-commensurate heterostructures and two-dimensional weakly bonded solids in the Materials Project database[140] of bulk materials. Their algorithm detected materials composed of 2D structures which were held together through weak bonds such as weakly ionic or van der Waals interactions and determined the dimensionality of van der Waals bonds between the subunits of bulk materials.

The algorithm also monitored the bonding length as a criterion to differentiate covalent and van der Waals bonds, in order to identify how atoms are connected in subunits. Based on this data mining investigation, 23 distinct chemical families consisting of 1173 2D materials with unique chemical formulas were identified while 325 of them were highlighted as potential 2D piezoelectric monolayers owing to the lack of an inversion centre in their single layer crystal structures and non-zero band gap, as described in Fig. 9c, d and 3. 943 out of the total 1173 2D materials have been experimentally synthesized.[48]

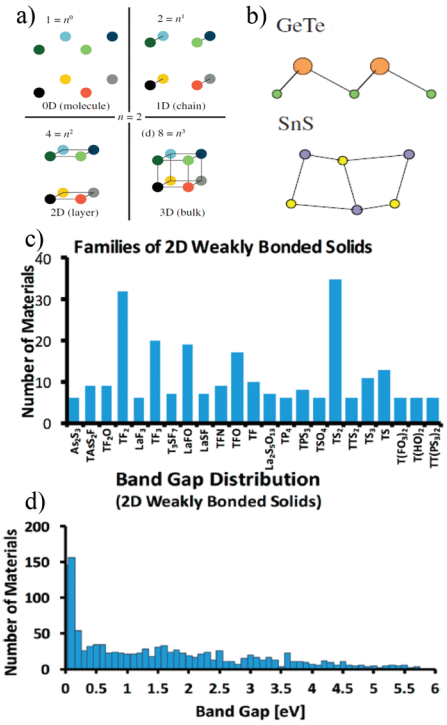

Fig. 9 (a) Illustration of a topology-scaling algorithm to find probable materials with layered motifs in their crystal structures. Black circles imply the cluster of bonded atoms in a unit cell while coloured circles represent seven periodic images of the same cluster for a 2 × 2 × 2 supercell of the original cell. Periodic images can bond to each other in 0, 1, 2 or 3 dimensions which define the dimensionality of structural motifs. (b) Buckled structures of GeTe and SnS with broken inversion symmetry that leads to piezoelectricity. Reprinted figure from ref. 98. Copyright (2017) by the American Physical Society. (c) Different groups of weakly bonded solids with 2D subunits and similar chemical compositions found through data mining in the Materials Project database (T: transition metal, Ac: actinides, F: halogens, As; large pnictogens, S: chalcogens and La: lanthanides). (d) Distribution of band gaps for bulk materials consisting of 2D layers estimated by the Kohn–Sham DFT calculation. Reprinted with permission from ref. 48. Copyright (2017) American Chemical Society.

4.1.1. Density functional theory. DFT has been employed to scrutinize and measure the properties of 2D materials, such as exfoliation energy, band gap, point group, and optical, physical and piezoelectric properties, and has been proven to be a robust technique.[97,98,141,142] DFT simulations also provide the opportunity to predict and explain the origin of piezoelectricity and compare the piezoelectric coefficients of different materials.[37,143] First principles DFT calculations indicated the presence of intrinsic piezoelectricity and strong piezoelectric coefficients in group-III monolayer monochalcogenides with an MX stoichiometry (M = Ga or In, X = S or Se).[41] Fig. 10a shows the atomic structure of 2D GaS from top and side views which is also the representative structure for GaSe and InSe monolayers. DFT-optimized parameters and their corresponding experimental structural parameters of bulk phases including monolayer thickness h, lattice constant a_0, band gap E_{gap} and M–M bond length d_{M-M} are listed in Table 2 for the

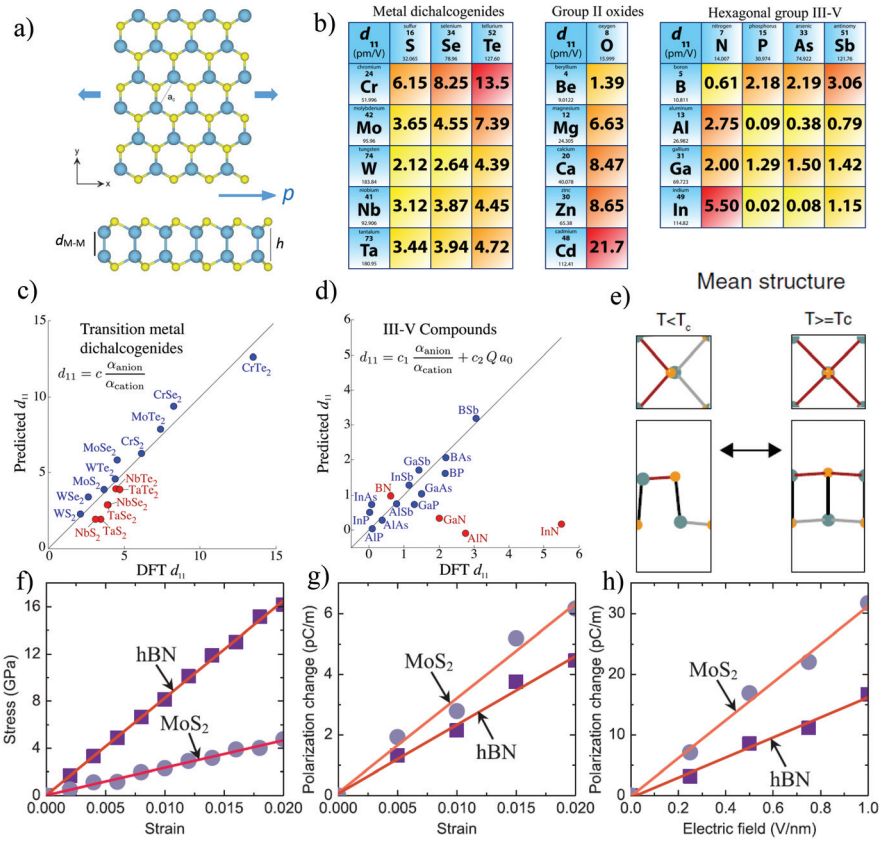

Fig. 10 (a) Top and side views of the GaS monolayer. Lattice constant, thickness of the monolayer and the distance between two bonded metal atoms are marked with a_0, h and d_{M-M}, respectively. The x and y directions correspond to the armchair and zigzag directions of the monolayer, respectively, and the bottom arrow indicates the polarization direction after uniaxial stretching of the monolayer. Reproduced from ref. 149. CC BY 4.0. (b) Periodic trend of d_{11} in 37 two-dimensional materials within three categories of metal dichalcogenides, metal oxides, and group III–V semiconductors (except PbO which possesses an inversion centre and a null piezoelectric response). (c) Direct relation of d_{11} in 2D transition metal dichalcogenides (groups 5 and 6) to the ratio of anion and cation polarizabilities. (d) In group III–V compounds, d_{11} is directly correlated to the anion and cation polarizabilities ratio and the Bader charge and in-plane lattice parameter, except for AlN, InN and GaN. Reprinted with permission from ref. 37. Copyright (2015) American Chemical Society. (e) 2D structural transition from a rectangular unit cell with threefold coordinated atoms to a square unit cell with fivefold coordinated atoms in SnS and GeSe monochalcogenide monolayers at T_c. Reprinted figure from ref. 150. Copyright (2003) by the American Physical Society. Molecular dynamics numerical measurements of (f) stress–strain, (g) polarization density–strain and (h) polarization density–electric field of 2D h-BN and MoS_2 (symbols). The elastic constant, piezoelectric coefficient and dielectric constant for 2D h-BN and MoS_2 (lines) were obtained by applying linear curve fitting on the corresponding results of MD simulations. Reprinted from ref. 151, copyright (2019), with permission from Elsevier.

direct comparison of DFT results and experimental parameters. The DFT calculations estimated that GaSe, GaS and InSe monolayers present significant piezoelectric coefficients (2.30, 2.06 and 1.46 pm V^{-1}, respectively) with the same order of magnitude as those of 2H-MoS_2 and h-BN indicating that a large piezoresponse can be observed in many 2D materials with a broken centrosymmetry.[41] Other studies have also predicted piezoelectricity in graphene oxide and doped graphene. DFT calculations estimated the piezoelectric coefficients to be 0.24, and 0.30 pm V^{-1} for graphene oxide and doped graphene, respectively.[29,39,144]

An intensive theoretical study was carried out by Blonsky *et al.*[37] on 37 2D materials from different families of metal oxides (MO, M = Be, Ca, Cd, Mg, Pb, Zn), metal dichalcogenides (MX_2, M = Cr, Mo, Nb, Ta, W and X = S, Se, Te) and group III–V semiconductors (AX, A = Al, B, Ga, In and X = As, N, P, Sb) to determine their piezoelectric coefficients. All of these materials showed a hexagonal symmetry and nonzero piezoelectricity, as shown in Fig. 10b, and the majority of them exhibited d_{11} coefficients higher than the value for typical bulk

Table 2 The comparison of the structural parameters and band gaps of bulk and monolayer materials obtained through experiments[145–148] and DFT calculations,[41] respectively (a_0, h and d_{M-M} are in Å and E_{gap} is in eV). Reproduced with permission from ref. 41

	Bulk				Monolayer			
Material	a_0	h	d_{M-M}	E_{gap}	a_0	h	d_{M-M}	E_{gap}
GaS	3.59	4.60	2.45	2.59	3.64	4.66	2.48	2.37
GaSe	3.76	4.78	2.46	2.10	3.82	4.83	2.47	1.81
InSe	4.00	5.28	2.78	1.17	4.09	5.39	2.82	1.40

Table 3 Piezoelectric coefficients (d_{11} in pm V^{-1} and e_{11} in pC m^{-1}) and formation energies (ΔE_f in meV per atom) for 2D metal dichalcogenides, group II oxides and group III–V compounds. Reprinted with permission from ref. 37. Copyright (2015) American Chemical Society

Metal dichalcogenides				Group II oxides				Group III–V compounds			
Material	d_{11}	e_{11}	ΔE_f	Material	d_{11}	e_{11}	ΔE_f	Material	d_{11}	e_{11}	ΔE_f
CrS_2	6.15	543	75	BeO	1.39	132	90	BN	0.61	139	90
$CrSe_2$	8.25	575	75	MgO	6.63	230	430	Bp	2.18	240	520
$CrTe_2$	13.45	654	85	CaO	8.47	155	560	BAs	2.19	204	520
MoS_2	3.65	362	77	ZnO	8.65	266	190	BSb	3.06	206	590
$MoSe_2$	4.55	383	80	CdO	21.7	333	260	AlN	2.75	223	510
$MoTe_2$	7.39	467	83	PbO	0	0	85	AlP	0.09	3.5	520
WS_2	2.12	243	77					AlAs	0.38	12.7	500
WSe_2	2.64	257	80					AlSb	0.79	19.9	480
WTe_2	4.39	323	120					GaN	2.00	148	420
NbS_2	3.12	211	93					GaP	1.29	52.6	450
$NbSe_2$	3.87	222	97					GaAs	1.50	49.0	410
$NbTe_2$	4.45	184	100					GaSb	1.42	33.2	390
TaS_2	3.44	267	87					InN	5.50	224	450
$TaSe_2$	3.94	250	90					InP	0.02	0.5	440
$TaTe_2$	4.72	207	140					InAs	0.08	1.7	410
								InSb	1.15	17.9	380

piezoelectric structures, except 2D tetragonal PbO which has an inversion centre and a null piezoelectric tensor. In particular, CaO, CdO, $CrSe_2$, $CrTe_2$ and ZnO systems revealed remarkable piezoelectric coefficients, as listed in Table 3. The nominated 2D materials generally presented low formation energies compared to their bulk counterparts which facilitate their exfoliation from bulk structures[13,132] and some of them have already been synthesized and experimentally characterized.[20,152,153] Through DFT calculations, Duerloo *et al.*[29] discovered that unlike their bulk counterparts, many regular 2D monolayers of TMDCs possess piezoelectric properties. Their calculations of the piezoelectric coefficient of monolayer materials revealed that some of them may exhibit a piezoelectric coupling factor larger than many recognized bulk wurtzite structures such as AlN.[29]

Furthermore, the DFT calculation was used for finding a correlation between the piezoelectric coefficient and structural properties of these 2D materials. As shown in Fig. 10c, the piezoelectric coefficients (d_{11}) of 15 materials in group 5 and 6 transition-metal dichalcogenides are directly proportional to the ratio of polarizabilities of isolated cations and anions indicating that the strong piezoelectric coefficient in dichalcogenides arises from the small cation and large anion polarizability. A similar trend was identified in the case of 2D materials of groups III–V (Fig. 10d). In this class, piezoelectricity originates from the displacement of ions and the resulting change in polarization. It was observed that the piezoelectric coefficient is correlated to the ratio of cation and anion polarizabilities, and the formation of the Bader charge and lattice parameters.[37]

4.1.2. Molecular dynamics. MD is one of the main approaches to study nanomechanics, since the size-dependent properties in nanostructures can be well predicted through MD simulations using continuum theories.[154] MD calculations[155,156] have been employed sporadically for studying the origin of piezoelectricity and some other piezoelectric properties such as the piezoelectric coefficient, strain effects, and phase transition in the bulk and one-dimensional piezoelectric materials;[157–161] however, very few similar studies on 2D piezoelectric materials have been reported.[162]

MD has been used for predicting the fundamental effects of temperature on the physical properties of few-layered group-IV monochalcogenides, identifying temperature as an avenue towards the tuning of the material's properties. According to the MD calculations, SnSe and GeSe monochalcogenide monolayers experience a two-dimensional rectangular-to-square unit cell phase transition at a critical temperature T_c, as shown in Fig. 10e,[150] which leads to a dramatic change in their band structure and electronic, piezoelectric, spin and optical properties. Similarly, another MD simulation on the stability of 2H single-layer CrS_2 at 600 K showed no structural transition, indicating the stability of single-layer piezoelectric CrS_2 at this temperature.[143]

Recently, Zhang conducted MD simulations on the piezopotential properties of 2D h-BN and 2H-MoS_2 nanosheets.[151] Accordingly, a new nonlocal electromechanical model based on Eringen's nonlocal theory was designed for studying the small-scale effects in the analytical modelling of these 2D materials. The numerical simulations and analytical modelling showed that small-scale effects can change the electromechanical behaviours of 2D piezoelectric materials and significantly affect their piezopotential properties, indicating that previously used classical electromechanical models are not reliable for the precise characterization of the piezopotential in 2D piezoelectric materials. Moreover, the elastic constant, piezoelectric coefficient and dielectric constant of 2D h-BN and MoS_2 materials were numerically measured through the MD simulations, as shown in Fig. 10f and g. The MD findings also showed that the piezo-potential coefficients of both h-BN and 2H-MoS_2 nanosheets increased by decreasing their lengths which proves that the piezo-potential properties of 2D materials can be significantly enhanced at the nanoscale by

small-scale effects that change the electromechanical behaviours of 2D materials.[151]

4.1.3. Molecular structural mechanics. Although the material characteristics and element sectional parameters are readily available in material data handbooks or can be calculated through the element sectional dimensions for practically-produced macroscopic structures, there is no information about the sectional and elastic properties of atom–atom bonds for nanostructured materials; hence, establishing a link between the macroscopic structure and microscopic computational chemistry seems necessary.[43] For this purpose, the covalent bonds among two adjacent atoms act as connecting beam members with round cross-sections where individual atoms act like the joints of related load-bearing beam members with bending and axial stiffness and torsional rigidity. The sectional properties of these beam members are determined by setting a linkage between molecular mechanics and structural mechanics.[163,164] Subsequently, the whole nanostructure is considered and simulated as a space frame structure, which can be solved and explained by the MSM method.[43] MSM simulations have been extensively employed for the prediction and modelling of the mechanical behavior of different nanostructures such as graphene and h-BN nanosheets[165,166] and the study of piezoelectricity in 2D h-BN.[167] Using MSM, Zhang *et al.*[167] studied the buckling and pre-buckling deformation behaviors of h-BN nanosheets subjected to an electric field. These deformations are the consequence of the stress generated in the sheets through the reverse piezoelectric effect under the exposed electric field. The obtained results indicated structural selective deformations for BN as axial and shear deformations were observed in zigzag and armchair h-BN planes, respectively, suggesting the high dependence and relation of polarization in the BN nanostructure to the crystal orientation. The influence of the aspect ratio a/b of BN nanosheets on the critical buckling axial electrical field (E_{cr}) was also tracked by MSM. Calculations showed that E_{cr} decreases by increasing the ratio a/b, especially for armchair h-BN.

4.2. Experimental assessments

Generally, piezoelectric coefficients in piezoelectric materials can be determined through the direct measurement techniques such as laser Doppler vibrometry,[168,169] laser interferometry,[170] and pneumatic pressure rig,[171] by indirect methods including impedance and return loss[172] and acoustic wave[173] and by other methods.[174] However, most of these methods are unable to identify the local electromechanical properties at the nanoscale.

Moreover, by reducing the dimensions of piezoelectric materials to the atomic scale, the common characterization methods of measuring piezoelectricity in bulk materials such as the Sawyer–Towler-circuit method are not suitable and new alternatives were developed. Various techniques are used for the structural and elemental characterization of 2D piezoelectric materials and their outcomes are employed as inputs for either first-principles calculations and further simulations. The synthesis–structure–property correlations in piezoelectric materials can be established by comparing the results of these simulations and experimental measurements of the tested specimen.[8]

4.2.1. Piezoresponse force microscopy. PFM employs the inverse piezoelectric concept to measure piezoelectricity in materials. Basically, a small AC voltage is applied to the surface of the sample through the atomic force microscope (AFM) tip resulting in an inhomogeneous electric field below the tip. This electric field induces local surface deformations, including lateral torsions and vertical expansions or retractions which deflect the cantilever which is sensed by the lock-in amplifier.[175,176] The mechanism of PFM imaging and possible movements of the cantilevers are demonstrated in Fig. 11a

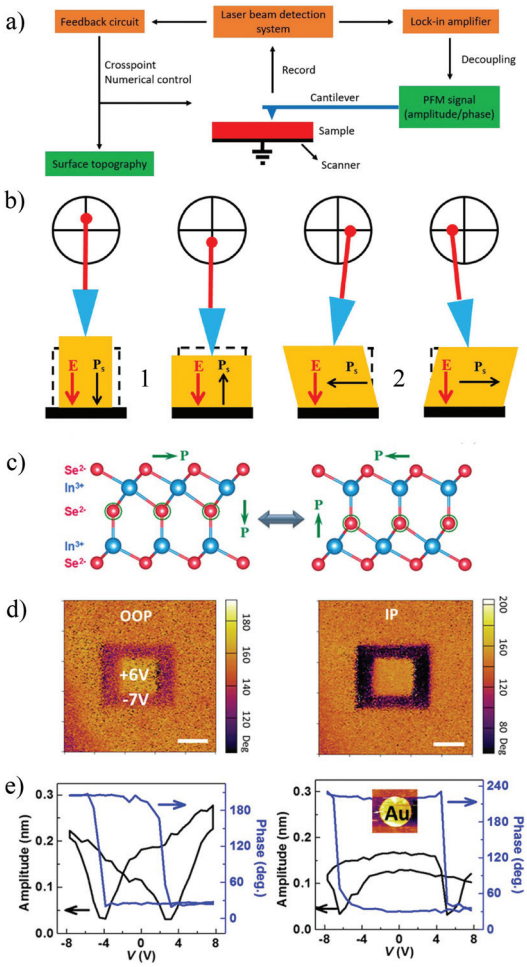

Fig. 11 (a) Illustration of the PFM mechanism. (b) Schematics of vertical (1) and lateral (2) PFM. Reprinted with permission from ref. 177. (c) In-plane (IP) and out-of-plane (OOP) switching coupling models in an In_2Se_3 flake. (d) OOP and IP phase images of the In_2Se_3 flake after writing two square patterns indicating that the polarization direction can be changed by an external bias. Scale bar is 1 μm. (e) Local ferroelectric switching loops of the In_2Se_3 flake without and with a Au top electrode. The butterfly-like amplitude–voltage loop and sharp change in the phase graph are typically observed in ferroelectric materials. Reprinted with permission from ref. 83. Copyright (2018) American Chemical Society.

and b.[177,178] The amplitude and phase of the generated deformations are used for identifying the strength and direction of dipoles in piezoelectric materials. Due to the improvement of the spatial resolution of PFM in recent years, the technique has become one of the most useful tools for characterizing the electromechanical properties of piezoelectric and ferroelectric nanostructures, allowing the characterization of domain nucleation and evolution,[179] the conduction of static domain imaging[180] and resolution analysis,[181] and manipulation and fabrication at the nanoscale.[174,182] The PFM technique is widely used for the quantitative measurement of piezoelectric coefficients, ferroelectric domain imaging and determining the domain switching behaviours in 2D piezoelectric materials. The image contrast arises due to changes in the piezoresponse sign when crossing the boundary of domains with opposite polarizations. As a special class of piezoelectric materials, ferroelectric materials present piezoelectricity due to the lack of structural symmetry. Ferroelectrics exhibit spontaneous polarization, *i.e.* polarization in the absence of an electric field; hence PFM is also employed extensively for studying ferroelectric materials. The ferroelectric nature of materials can be further confirmed by combining the amplitude–voltage butterfly loop, 180° phase-voltage reversal loop and switched domains caused by opposite voltages, as shown in Fig. 11c–e.[36,83]

4.2.2. Laser Doppler vibrometry. The out-of-plane vibrations with ultra-high frequencies can be detected by laser Doppler vibrometry (LDV).[183] Basically, the Doppler frequency shifts by light scattering on the moving surface. The shift in the Doppler frequency is directly proportional to the velocity of the surface and hence the non-contact and easy measurement of the surface vibration velocity is possible by tracking the Doppler frequency shift. An optical microscope can be used to transmit and focus the laser beam on the sample, as well as tracking the sample changes.[183] LDV has been used for measuring the piezoelectric coefficient of piezoelectric thin films of materials such as PZT, AlN, $LiNbO_3$, and NBT.[184–187] In such processes, a variable DC bias voltage and an alternating small voltage (V_{ac}) are applied to the piezoelectric material for measuring the piezoelectric hysteresis loop. An electric field is generated and cycled in the piezoelectric material and the resulted displacements are monitored. The DC bias field is applied in cycles to obtain the d_{33} *versus* electric field hysteresis loop and the piezoelectric coefficient can be calculated using the equation $d_{33} = \Delta t/V_{ac}$, where Δt is the amplitude of vibration (pm) of the piezoelectric material.[168] LDV has been employed to record the visual surface displacements of 2D MoS_2 attributed to the acoustically generated electric field in the piezoelectric MoS_2 monolayer, as shown in Fig. 12a.[169] Using the contrast against the substrate the piezoelectric coupling coefficient could be estimated.

4.2.3. Second-harmonic generation. Second harmonic generation (SHG) or frequency doubling is a special phenomenon of sum-frequency generation. SHG is described as a nonlinear optical technique in which a nonlinear material interacts with two photons of the same frequencies (ω), generating a new photon with twice the frequency (equivalently twice the energy)

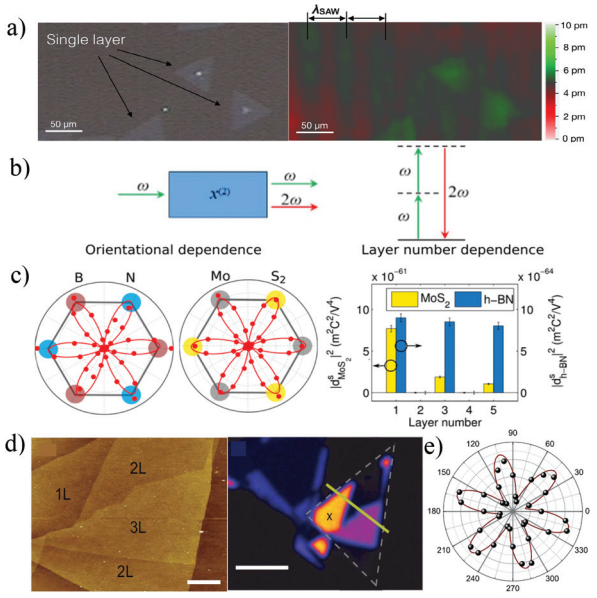

Fig. 12 (a) Optical image of 2D MoS_2 flakes (left) and visual evidence of their inherent piezoelectricity by measuring the vibration pattern and intensity in single layer MoS_2 flakes by laser Doppler vibrometry (LDV) after acoustic wave excitation (right). Reprinted with permission from ref. 169. Copyright (2016) American Chemical Society. (b) Description of second-harmonic generation and schematic energy-level diagram. (c) Fitted curves of the second-harmonic (SH) intensity of odd-layer atomically-thin h-BN and MoS_2 samples as a function of their crystallographic orientation. Column diagram shows the layer dependence of the SH intensity and surface nonlinear susceptibility in few layered (one to five) MoS_2 and h-BN materials indicating the noncentrosymmetric structure of odd layer thicknesses. Reprinted with permission from ref. 23. Copyright (2013) American Chemical Society. (d) AFM image of a MoS_2 thin film with a variable thickness from 1 layer to 3 layers (scale bar is 1 μm) and the corresponding second-harmonic image where the brighter color indexed by X means a stronger SHG intensity in the 1L region of MoS_2 (scale bar is 5 μm). (e) Polar plot based on the second-harmonic intensity as a function of the angle in the MoS_2 monolayer. Reprinted figure from ref. 190. Copyright (2013) by the American Physical Society.

and half the wavelength of the original photons, as depicted in Fig. 12b. Similar to other even-order nonlinear optical cases, SHG is not found in materials with inversion centrosymmetry; therefore it can be applied as a powerful tool for the characterization of ferroelectric and piezoelectric materials.[188,189] SHG has been used widely as a robust method to probe the symmetry variations in 2D piezoelectric materials and for domain imaging and switching in ferroelectrics.[14,190,191] The optical second-harmonic generation in few-layered (one to five) atomically-thin MoS_2 and h-BN samples was investigated by Li *et al.*[23] As shown in Fig. 12c, strong and weak SHG signals were observed in odd and even layers, respectively, implying the noncentrosymmetric structure and broken inversion symmetry of materials with odd layer thickness. Rotational symmetries of lattices were also revealed by measuring the SHG as a function of crystal orientations in odd layer MoS_2 and h-BN samples which proved that few-layered MoS_2 and h-BN materials possess the same crystallographic structure as those of the layers in

their bulk crystals. In a similar manner, the orientational dependency of SHG has been used for imaging the crystal domains of CVD-grown and exfoliated 2D MoS_2.[190,192] An example is shown in Fig. 12d, in which the brighter region presents a stronger second-harmonic intensity in the MoS_2 monolayer which depends on the laser input power and the crystal rotation angles. A sixfold pattern can be obtained when the second-harmonic intensity of this area (1L MoS_2) is plotted as a function of the rotation angle shown in Fig. 12e. PFM and SHG are considered as ideal non-destructive techniques for the characterization of thin films. The extreme sensitivity of SHG to symmetry changes also leads to its application in the determination of the Curie temperature and the identification of ferroelectric–paraelectric phase transitions.[193] However, PFM offers a remarkably higher spatial resolution in comparison with SHG which allows high resolution domain imaging. As such a combination of both techniques is often applied.[36]

4.2.4. Direct tensile testing. Tensile testing and lateral bending are known to be the most common ways of determining direct piezoelectricity by measuring the generated electric potential or charge under mechanical deformation in piezoelectric nanostructures; however, the low amplitudes of the generated charges or voltages in 2D materials and the need for ultrasensitive electronic measurement devices present challenges.

In the direct tensile testing method, the piezoelectric specimen is laid on a precision tensile device, while two conductive contacts are created at the specimen's sides which are linked to a charge amplifier. Due to the piezoelectric effect, the applied direct tensile stimuli induce electric polarization in the sample and the generated electric charges are measured.[8] According to the experimental tensile study on monolayer MoS_2 by Wu *et al.*,[14] oscillating current and voltage signals are observed when odd-layer MoS_2 materials are stretched and released, as shown in Fig. 13a and b. Positive voltage and current output were identified when a strain was applied in the x direction (armchair), while a decreasing strain resulted in a negative output which directly indicated the conversion of mechanical stimuli into electricity by 2D MoS_2. By straining the device along the armchair direction of MoS_2, strain-induced piezoelectric polarizations evolve in the zigzag edges of the sample and a flow of electrons occurs in an external load resistor. Here, by releasing the device into its initial state, piezoelectric polarization charges disappear and electrons drive back in the opposite direction. Stretching and releasing cycles of the device cause alternating pulses. However, by the rotation of the strain direction from x (armchair) to y (zigzag), the piezoelectric response is reversed. This dependency of piezoelectric charge polarization on the strain directions can be interpreted through the symmetry analysis of the D_{3h} point group of single layer MoS_2.

According to the D_{3h} symmetry, 2D MoS_2 only presents one non-zero independent coefficient e_{11}. Thus, the in-plane polarization along the x direction can be explained as $P_1 = e_{11}(\epsilon_{11} - \epsilon_{22})$, where ϵ_{11} and ϵ_{22} are the strain tensors along the x and y directions, respectively. Consequently, the sign of the piezoelectric output reverses by switching the strain direction from

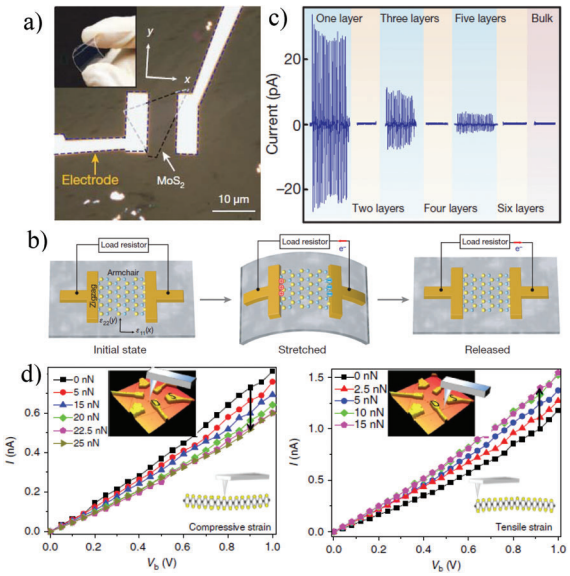

Fig. 13 (a) Optical image of a typical device made by depositing a single layer MoS_2 flake on a PET flexible substrate between metal electrodes. (b) Mechanism of generating the piezoelectric output due to continuous stretching and releasing of the 2D MoS_2 piezoelectric device. Piezoelectric polarizations are produced at the zigzag edges of the MoS_2 monolayer upon stretching. (c) Decreasing the piezoelectric output by increasing the number of layers in the MoS_2 flake while even layers and the bulk do not show any output. Reprinted by permission from Macmillan Publishers Ltd,[14] copyright (2014). (d) Electromechanical behaviour and I–V_b characteristics of a MoS_2 device under compressive (left) and tensile (right) strains at different applied forces. Inset photos present the relation between the locations of the applied forces and the resulting compressive/tensile strains. Current values decreased and increased under compressive and tensile strains, respectively. Reproduced from ref. 102. CC BY 4.0.

x (armchair) to y (zigzag).[14] In fact, a peak output of 20 pA and 15 mV associated with a mechanical to electrical energy conversion efficiency of 5.08% was produced after the MoS_2 monolayer was strained by 0.53%, while this output decreased with increasing thickness (Fig. 13c). The piezoelectric effect in triangular MoS_2 monolayers was also studied by measuring the I–V curves under isotropic mechanical deformation using an AFM tip in the centre and edge of 2D MoS_2. A drop and a growing trend in current magnitudes were observed under compressive and tensile strains on these MoS_2 monolayers, respectively, which were fixed between sets of S–D (source/drain) electrodes, as shown in Fig. 13d. These devices could be used as strain/force sensors. The contrasting behaviour of compressive and tensile strains was rationalized by differences in locally strain-induced charge polarizations.[102,194]

5. Applications of 2D piezoelectric materials

As discussed earlier, the polarization direction imposes a crucial impact on the piezoelectric properties of 2D materials

which subsequently defines their specific performance in different devices and applications. For example, although the h-BN monolayer presents good thermal conductivity and superior mechanical and chemical properties, its application is limited due to the planar structure and the absence of out-of-plane piezoelectricity.[2] Therefore, attempts have been made to predict and engineer different polarization directions in other 2D material candidates for nanoelectromechanical applications.[37,39,60,62,66,74,195] A symmetry analysis using density-functional perturbation theory predicted 37 2D materials with an in-plane (d_{11}) piezoelectric coefficient among metal oxides and metal dichalcogenides, while an additional out-of-plane coefficient (d_{31}) was found in some hexagonal group III–V materials, such as AlAs and InP.[37]

The exceptional and unique properties of 2D piezoelectric materials have led to the creation of many innovative devices for a large variety of applications such as piezotronics,[14,15,196] energy harvesting and storage,[14,197–200] catalysis,[138,201,202] optoelectronic,[20,203,204] nanoelectronic[205,206] and piezophototronic applications,[15,207,208] actuations,[209] sensing[210–212] and bio-applications.[213–215] The most important applications of 2D piezoelectric materials are discussed in the following section.

5.1. Piezotronics

The presence of piezoelectricity in semiconductor materials with different crystal structures has greatly helped in the development of the piezotronic research field.[216,217] The piezotronic effect was introduced for 3D wurtzite piezoelectric nanostructures in 2007[218] and since then many electronic devices such as strain sensors,[219,220] nanodiodes,[221] and nanotransistors emerged based on piezotronics.[222] This effect can be explained as the change of the interfacial carrier dynamics as a result of piezoelectric polarization modulation.[223] The piezotronic effect employs the piezoelectric potential as the gate voltage to modulate the properties of charges which affect the interfacial properties, in contrast with conventional electronics which rely on the electrostatic coupling between the electric field induced by the gate voltage and a conductive channel.[15] One of the very first experimental demonstrations of piezotronics in 2D materials has been in 2H-MoS_2 monolayers,[14] which were also confirmed by DFT calculations.[142,197] This first 2D piezotronic device was successfully implemented by transferring MoS_2 flakes on flexible polyethylene terephthalate (PET) substrates, as shown in Fig. 13a. The resulting metal–semiconductor–metal structure comprised of two back-to-back Schottky barriers. The effect of strain on the electrical transport properties of such MoS_2-based devices was investigated by Wu *et al.* and Liu *et al.*[14,142] They measured the electric current–voltage curves of the developed devices and assigned the asymmetry changes in the output curves to the presence of the piezotronic effect, which modulates the metal–MoS_2 contacts, as shown in Fig. 14a and b. It was found that under strains, the current–voltage curves showed alternating changes, indicating that changes in the transport behaviors mainly arise from piezotronics.

Since 2D MoS_2 is a semiconducting piezoelectric material, for which carrier transport can be modulated by strain-induced piezoelectric charges, it is a promising candidate for

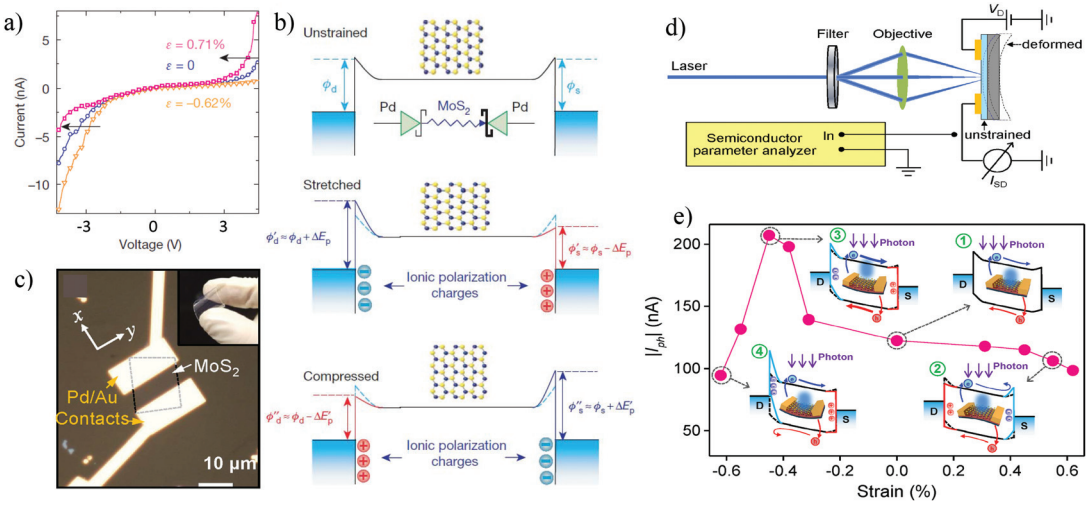

Fig. 14 (a) The effect of strain in a single-layer MoS_2 device under an opposite drain bias which leads to an asymmetric modulation of carrier transport implying the piezotronic characteristics of the device. The current–voltage curve moves under the applied strains (ε with negative and positive signs denotes the compressive and tensile strains, respectively). (b) The band diagrams of a single layer MoS_2 device. The observed piezotronic behaviour is explained based on the changes of Schottky barrier heights due to the strain-induced polarization, where ϕ_s and ϕ_d are the heights of Schottky barriers at source and drain contacts, respectively, and E_p represents the change in the Schottky barrier height as a result of piezoelectric polarization charges. Reprinted by permission from Macmillan Publishers Ltd,[14] copyright (2014). (c) Optical image of a flexible two terminal single-layer MoS_2 piezophototronic device. (d) Schematic description of the setup used for studying the piezophototronic properties of 2D MoS_2. (e) Band diagrams explaining the working mechanism of the piezophototronic process and the relation between the photocurrent (I_{ph}) and the applied strain in the monolayer MoS_2 photodetector. The observed piezophototronic response is attributed to the variations of the Schottky barrier height caused by strain-induced polarization. Reproduced with permission from ref. 208, copyright John Wiley and Sons, 2016.

developing piezotronic devices.[2] By assembling a strain/force sensor, Qi *et al.* investigated the piezotronic properties of 2D MoS_2 arising from coupled in-plane piezoelectricity and carrier transport.[102] In this work, local isotropic strains were applied to different spots of monolayer MoS_2 using a contact mode AFM, whilst an external bias was applied for measuring the corresponding conductivity changes. Here the AFM load on the centre and near the edges of the MoS_2 monolayer led to compressive strain (concave shaped deformation) and tensile strain (convex shaped deformation), respectively, as shown in Fig. 13d. With increasing force, the current decreased and it increased under compressive and tensile strains, respectively. The current modulation in this device was associated with the changes in the Schottky barrier height (SBH) as a result of the applied strains and piezotronic effect. In such a device, compressive strain increased the barrier height thereby decreasing the generated current. Conversely, a tensile strain decreased the barrier height and increased the current. At the molecular level, and according to the energy band diagrams, negative piezoelectric polarization charges are generated at the zigzag edges of the 2D MoS_2 triangle under compressive strain. The produced negative piezopotential depletes free electrons close to the metal interfaces, leading to increased SBHs at both contacts and eventually current reduction under the compressive strain. In reverse, positive piezoelectric polarization charges are induced at three zigzag edges of the MoS_2 monolayer due to a local tensile strain and the free electrons near the interfaces between metal contacts and MoS_2 are attracted by the produced positive piezopotential, resulting in reduced SBHs at both contacts and increase in the measured current under the tensile strain.[102] The ability of the piezotronic effect in the modulation of metal–semiconductor contacts in 2D materials introduces new approaches to develop photovoltaic, optoelectronic, catalysis and force nanosensor technologies[102] without the need for modifying the chemistry and physics of interfaces.

5.2. Data transfer and modulation/demodulation

One of the possible applications of piezoelectricity in 2D materials which are also semiconducting is the modulation/demodulation of the data. After the exposure of a direct bandgap 2D semiconductor to light, excitons are produced that can be dragged using acoustic waves along the planar surface of the 2D materials. The excitons only recombine when they are screened. The entrapment of the excitons on the surface and the presence of piezoelectricity help to alter the velocity of the propagation *via* the applied signals and as such provide the modulation and demodulation capability.[224] This was first demonstrated in monolayer MoS_2 and the concept should be further expanded to other 2D piezoelectric materials for commercial applications.[169]

5.3. Piezophototronics

Some 2D materials show unique photonic properties in addition to their remarkable piezoelectric abilities, leading to novel applications in innovative optoelectronics. The piezophototronic phenomenon is generated in 2D materials when distinctive piezoelectric, photonic and semiconductor properties are coupled.[15] Fundamentally, electro-optical observations such as carrier generation, separation, transport and recombination at p–n junctions or metal–semiconductor Schottky contacts can be systematically controlled by applying a strain-induced piezopotential in piezophototronic materials[218,225] leading to the emergence of improved optoelectronic devices including solar cells, light-emitting diodes (LEDs), photosensors and photoelectrochemical devices.[15,226–230] Both piezotronic and piezophototronic systems employ piezopotential as gate stimuli to modify the optoelectronic and electronic interactions in semiconductor devices.[231] The principles of the piezophototronic effect was initially explained in 2010 by Hu *et al.*[232] for 3D wurtzite piezoelectric nanostructures. This effect was also recently observed in 2D materials such as 2H-MoS_2 for applications in strain-gated flexible optoelectronics.[208] For this purpose, the crystallographic orientations of mechanically-exfoliated MoS_2 monolayers were determined through the second-harmonic generation method before transferring on flexible substrates between two electrical contacts, as shown in Fig. 14c. The piezophototronic performance of this 2D MoS_2-based device was monitored by measuring the generated photocurrent under systematically tuned optical illumination and mechanical strain, as depicted in Fig. 14d. The process of the strain-gated flexible optoelectronics and the strain dependence of the photocurrent in a device under a −2 V drain bias is schematically illustrated in Fig. 14e. By applying a mechanical strain to the device, the piezoelectric charges generated in the zigzag edges of the MoS_2 monolayer affect the metal–MoS_2 contacts directly through modulating the concentration or distribution of free carriers in single layer MoS_2 at the vicinity of the Schottky barrier. In another word, the mechanical strain acts as a controlling gate signal to modify the optoelectronic mechanism which can be called the piezophototronic effect. As shown in Fig. 14e, the tensile strain and large compressive strain caused a decrease in the photocurrent, while a small compressive strain increased the photocurrent, as discussed in ref. 208. The piezophototronic behavior of a 2D MoS_2 single Schottky solar cell was theoretically simulated and compared with other counterparts including $MoSe_2$ and WSe_2.[233] This study revealed that the performance of solar cells can be enhanced when the SBH is tuned effectively by strain-induced piezopolarization charges in the interface. Accordingly, an increase of 5.8% in the open-circuit voltage was seen after applying a 1% strain (Fig. 15a) and the modulation impact of the piezophototronic effect on the MoS_2 solar cell was found to be significantly higher than that of WSe_2 and $MoSe_2$ solar cells (Fig. 15b) likely due to the higher measured piezoelectric coefficient in MoS_2 (although theoretically the coupling coefficient of $MoSe_2$ is higher than that of MoS_2 – Table 3).[233]

5.4. Energy harvesting

2D piezoelectric materials are also of great interest in the construction of flexible nanogenerators, owing to their morpho-

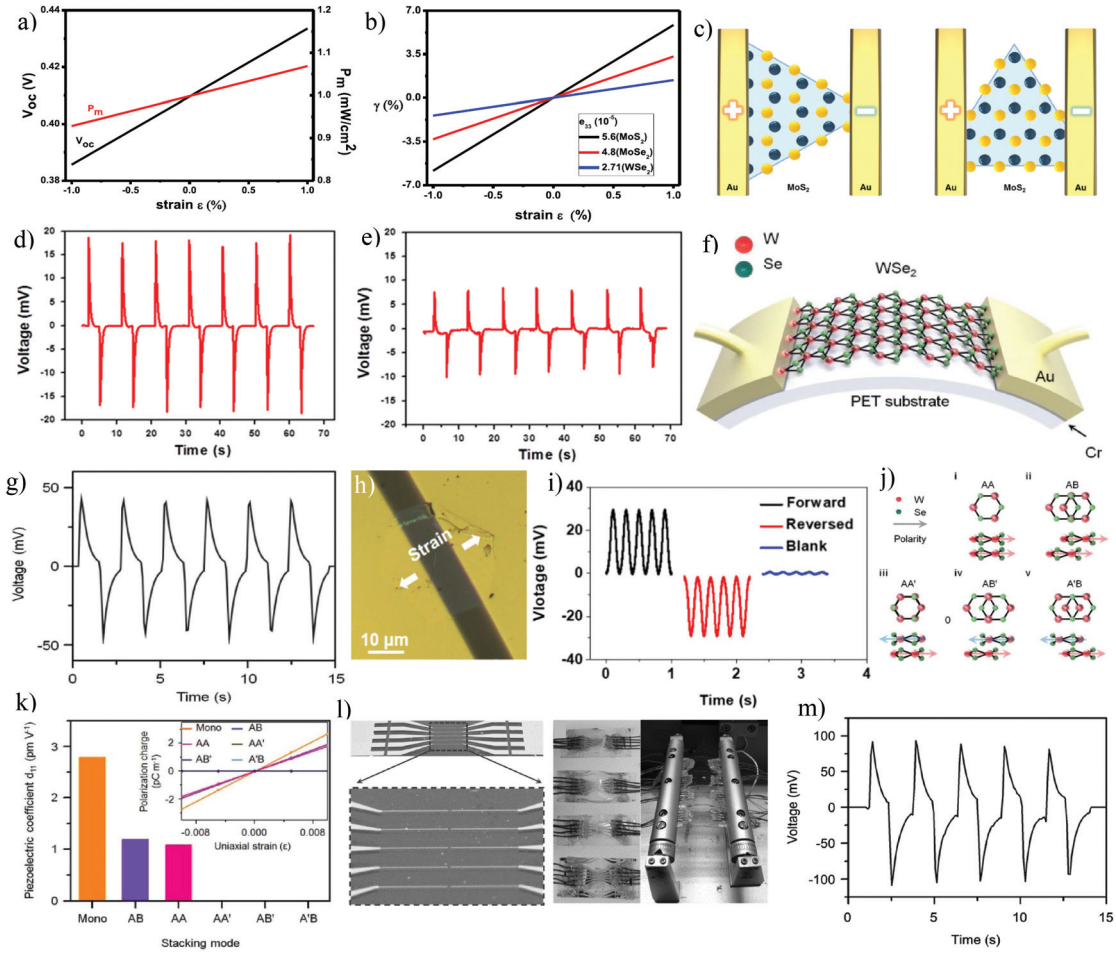

Fig. 15 (a) The dependence of open circuit voltage (V_{oc}) and maximum output power (P_m) under various applied strains in a two-dimensional MoS_2 piezophototronic solar cell. (b) The comparison of γ of a piezophototronic solar cell in three 2D materials (MoS_2, $MoSe_2$ and WSe_2) as a function of strain. The ratio γ introduces the modulation for the open circuit voltage of a piezophototronic solar cell by piezoelectric charges. Reprinted from ref. 233, copyright (2017), with permission from Elsevier. (c) Electric field applied to a MoS_2 monolayer along the armchair (Mo and S parallel, left) and zigzag (Mo and S in the same line, right) directions of the triangular monolayer MoS_2 flake. (d) Voltage output resulted by applying strain to the MoS_2 nanogenerator along the armchair and (e) zigzag directions. Reprinted from ref. 104, copyright (2016), with permission from Elsevier. (f) Piezoelectric energy harvester (PEH) based on the WSe_2 monolayer with the Cr/Au electrodes and PET substrate. (g) Voltage output signal of the 2D WSe_2-based PEH by applying a 1 GΩ external load. Reproduced with permission from ref. 234, copyright John Wiley and Sons, 2017. (h) A piezoelectric device based on a PbI_2 nanosheet connected to Au electrodes on a PET substrate. (i) Forward and reversed open-circuit voltages of a 2D PbI_2 piezoelectric device while the blue line indicates the open-circuit voltage of the device without a PbI_2 nanosheet. Reprinted from ref. 235, copyright (2018), with permission from Elsevier. (j) Different stacking structures of bilayer WSe_2; AA and AB stacking modes show polarity in the same direction while the directions of polarity in the AA′, AB′ and A′B stacking structures are opposite. (k) The comparison of simulated piezoelectric coefficients of monolayer WSe_2 with AA and AB stacked structures. The inset shows the estimated polarization charges obtained by DFT simulation for the WSe_2 monolayer compared to different stacking counterparts under the same uniaxial strain. (l) A large-area integrated PEH device created by parallel connection of four arrays of tb-WSe_2 (each array consists of five tb-WSe_2, as magnified in the left photo) and (m) the output voltage signals of this tb-WSe_2 based PEH device measured periodically under 1 GΩ of load resistance. Reproduced with permission from ref. 234, copyright John Wiley and Sons, 2017.

logical advantages.[1] As discussed earlier, the strong piezoelectricity with a d_{11} value in MoS_2 monolayers (Table 3) was used within a flexible substrate to form a 2D nanogenerator.[14] In contrast to this nanogenerator where the piezoelectric response was only found in the zigzag edges of MoS_2 monolayers, Kim *et al.* detected an electrical output on both zigzag and armchair edges of the triangular-shaped MoS_2 monolayer, and particularly the nanogenerator device based on the armchair direction of MoS_2 provided a double output power compared to the zigzag direction under the same strain of 0.48%, as demonstrated in Fig. 15c–e.[104] Following these pioneering studies on MoS_2 nanogenerators, other nanogenerators for energy harvesting based on 2D WSe_2[234] and PbI_2[235] were reported as shown in Fig. 15f–i. Although the previous report[23] indicated that nanomaterials with even layer thickness possess an AA′ stacking structure and consequently are non-piezoelectric due to the centrosymmetric structure, Lee *et al.* proved that piezoelectric properties can be engineered in WSe_2

bilayers (b-WSe_2) through turbostratic stacking and artificial transferring of the WSe_2 monolayer (m-WSe_2) onto another which results in tb-WSe_2 structures with another four stacking modes of AA, AB, A′B and AB′, as shown in Fig. 15j. Since the AA and AB modes of stacked b-WSe_2 exhibit polarity in the same direction, they retained the piezoelectric coefficients of 1.08 and 1.19 pm V^{-1}, respectively (Fig. 15k). In this work, the total output of tb-WSe_2 piezoelectric energy harvesters (PEHs) was increased by integrating a sequential series of tb-WSe_2 nanogenerators through a multi-electrode patterning design, as shown in Fig. 15l and m.[234] López-Suárez *et al.*[198] showed that tailored nonlinearities in 2D-based piezoelectric systems can also lead to remarkable energy harvesting from ambient energy inputs such as vibration and thermomechanical sources. They explored the dynamics and applications of wide bandgap h-BN monolayers in nonlinear vibration energy harvesting devices with the aid of *ab initio* calculations and molecular dynamics simulations. The system was driven into a nonlinear bistable situation by applying the compressive strain. In this regime, quasi-harmonic vibrations were combined with low-frequency swings between the minima of a double-well potential and electrical power is naturally produced in the nonlinear mechanical harvester due to the intrinsic piezoelectricity of 2D h-BN. In particular, it was predicted that a 20 nm^2 device (20 nm × 1 nm h-BN monolayer) under 0.3% compressive strain can generate up to 0.18 pW from a 5 pN vibration. Such a device has yet to be experimentally shown.

5.5. Sensors

2D piezoelectric materials are employed as constituents of different types of sensors such as strain, optical, humidity, chemical, and gas sensors. Fabrication of strain sensors requires materials with specific characteristics such as excellent electrical performance, good mechanical compliance and suitable processability that allow patterning for device fabrication. So far 1D nanomaterials, including nanowires and nanorods of piezoelectric materials such as ZnO, have been used as the building blocks of strain sensors.[219] However, fabrication of such 1D piezoelectric sensors on a large scale is challenging due to difficulties with picking up and placing nanorods across electrodes. Since the dimensionality of 2D piezoelectric materials and layered semiconductors is compatible with the large-scale microfabrication techniques of thin films, they do not show the limitations of 1D materials. A superior gauge factor of ~760, higher than those for silicon (~200) and graphene (~300) strain sensors, was characterized for a 2D-based MoS_2 strain sensing device, suggesting the potential of MoS_2 monolayers for highly sensitive strain sensing. The higher sensitivity and gauge factor of MoS_2 monolayers were attributed to enhanced piezoelectric polarization in 2D MoS_2.[14]

Using ZnO nanoplatelets, Liu *et al.*[237] reported a new kind of 2D piezotronic transistor (2DPT) with a very high pressure/sensitivity between 60.97–78.23 meV MPa^{-1} which is much higher than that of nanowire-based piezotronic transistors. In addition, by ordered assembly of ZnO nanoplatelets, a 2DPT array with an unprecedented spatial resolution of 12 700 dpi for piezotronic transistors was obtained. This study demonstrated the advantage of ZnO 2DPT as an active sensor for high-resolution tactile sensing. 2D materials with the piezophototronic effect also have been developed for optoelectronic applications such as photodetectors for optical sensors.[208]

5.6. Actuators

Actuators are used for producing mechanical vibrations and motions to move or control a system by utilizing the reverse piezoelectric effect and applying a bias voltage. Materials with nanometric dimensionalities introduce extreme strength mechanical responses. Nanometer-thick layers compared to bulky structures present enhanced strength and additional functionalities for applications in elastic strain engineering (ESE) due to efficient strain transfer, easy integration and feasible processing. In particular, 2D materials depict a unique high stretchability up to ~20% strain magnitudes promoting their use for ESE.[209] The modulation of strain in piezoelectric actuators has been used for tuning the physical properties of different materials such as 2D semiconductors, superconductors, ferromagnets and quantum dots.[238]

Actuations in 2D piezoelectric materials can be investigated by theoretical simulations for better understanding of the vertical piezoelectric experimental results. For instance, COMSOL Multiphysics simulation can be used to estimate the deformation of such 2D films under the applied voltages. Simulations have shown that ultrathin piezoelectric CdS might generate an expansion up to 150 pm under a negative voltage of −5 V, as shown in Fig. 16a–c.[54] Actuators can be used for assessing the physical parameters of interest in 2D piezoelectric materials. For example, the PFM amplitude mode can probe an out of plane (vertical) piezoresponse in piezoelectric ultrathin films.[54] Tunable biaxial stresses were applied on a graphene monolayer using a piezoelectric actuator to study the characteristic Raman features of graphene.[236] An electromechanical device comprising single layer graphene (SLG) integrated on the piezoelectric $[Pb(Mg_{1/3}Nb_{2/3})O_3]_{0.72}$-$[PbTiO_3]_{0.28}$ (PMN-PT) substrate was produced for smooth variations of strain by tensile stress or biaxial compression to graphene, as shown in Fig. 16d. The optical and photoluminescence properties of 2D WSe_2 [239] and tri-layer MoS_2 [240] were also investigated through the same approach.

5.7. Biomedical applications

Flexible electronics, in particular lead-free biocompatible piezoelectric materials, offered many promises in bioscience for applications in biomedical devices, nanogenerators, sensors, bioinspired artificial skins and many more.[31,131,241–243] 2D TMDC nanosheets, which also belong to the family of piezoelectric materials when they are in monolayer morphology, are being used widely in biomedical research due to their excellent characteristics such as large surface-to-volume ratio, ease of surface modification, good cytocompatibility, high thermal and optical conversion efficiency and strong spin–orbit coupling.[213] Indirectly, by reducing the power consumption of biomedical and portable

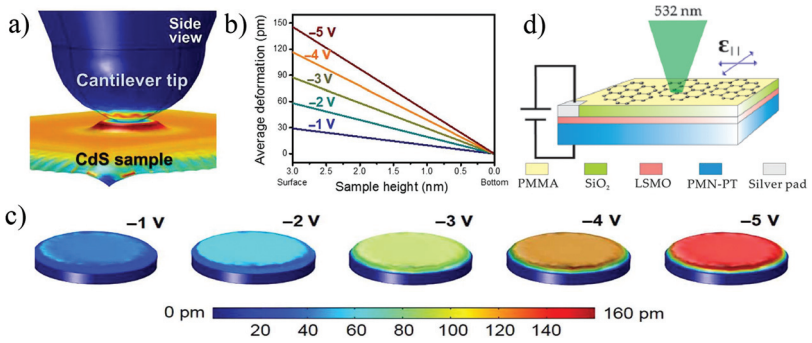

Fig. 16 (a) Side view of the stress distribution and deformation of a CdS thin film under the applied voltage induced by a PFM tip. (b, c) Linear increment of deformation and expansion of the CdS thin film from ~30 to ~150 pm when the applied DC voltage varies from –1 V to –5 V on the surface indicating a high vertical piezoelectricity in the CdS ultrathin film as an actuator. Adapted with permission from ref. 54, copyright American Association for the Advancement of Science, 2016. (d) The schematic illustration of a thin actuator used for applying electromechanical in-plane biaxial strain to graphene. Reprinted with permission from ref. 236. Copyright (2010) American Chemical Society.

electronic devices, the power generated by harvesting electrical energy from human activities or biomechanical movements, such as muscles and cardiac/lung motions, can be used for powering these devices or stored in batteries for self-powered wireless sensors.[244–246] These energy harvesters consist of organic or inorganic piezoelectric materials embedded in stretchable and flexible thin films such as polyimide (PI), polyethylene terephthalate (PET) and polydimethylsiloxane (PDMS).[1] As discussed earlier, ultra-sensitive and high-performance 2D piezoelectric materials such as MoS_2 [14,104] and WSe_2 [234] are employed as the main building blocks of nanogenerators which can also be used in biomedical applications.[1,242,245]

6. Conclusion and future perspective of 2D piezoelectric materials

All in all, even one century after of the discovery of piezoelectricity, many concepts of this phenomenon have remained unknown and recent developments of piezoelectricity in 2D materials have provoked much more in-depth research in this field. In fact, fascinating properties have been shown to exist at the 2D scale since many non-piezoelectric forms of bulk materials become piezoelectric by downsizing to the single or few fundamental layers due to the disruption of inversion centres and broken centrosymmetry. The planar surface of 2D materials exposes all of the structural constituents for efficient surface modification to enhance the piezoelectric properties even further.

The thickness reduction to the atomic level induces unique properties in 2D piezoelectric materials which are important for exploring the interactions between free charge carriers, phonons and photons. Furthermore, the limited number of atoms and the simple structural design of typical 2D materials provide an uncomplicated framework for computational analyses and simulations as robust tools for understanding the fundamental atomic interactions and designing novel materials. Extensive efforts have been focused on the screening of 2D nanostructures, and both experimental results and computational predictions consistently confirmed the intriguing properties of 2D piezoelectric materials for innovative electronic devices and nano-electromechanical systems.

The intrinsic piezoelectricity has been predicted in diverse 2D materials, while most of them have not been determined experimentally due to their instability and limitations of synthesis methods; thus novel and controllable synthesis techniques need to be devised towards the ideal preparation of 2D piezoelectric materials that can also accommodate suitable carrier concentrations. Furthermore, more chemically stable 2D piezoelectrics have to be considered through theoretical studies and simulations, with a special focus on their availability and stability in an ambient environment. Although 2D piezoelectric materials demonstrate outstanding piezoelectric coefficients with the same order of magnitude, larger than those of their bulk counterparts, these values are lower than those of some high-performance and well-known bulk piezoelectric materials such as PZT. In this regard, attention should be diverted to those 2D crystals such as PbO and SnS that have been predicted to possess colossal piezoelectric coupling coefficients in monolayers. Several key features of piezoelectric materials such as piezoelectric coefficient, polarization value and Curie temperature should be measured quantitatively to provide a clear comparison between 2D piezoelectric materials and other morphologies. The generation of piezoelectricity by surface modification has been dominantly invested on graphene[247] while piezoelectricity could be tailored for various monolayer materials such as carbon nitride,[248] phosphorene,[249] germanene[250] and silicone[251] by surface engineering. As another promising view, 2D piezoelectric materials can be used as the building blocks of innovative van der Waals heterostructures and 2D material composites.

Efficient theories and modelling frameworks need to be developed for better understanding of 2D piezoelectric materials' behaviors observed in experiments and simulations; in particular, the nonlinear relations between the electrome-

chanical coupling effect and the applied strain in 2D piezoelectric materials have to be taken into the account since it has been proven that these nonlinearities play critical roles in the electromechanical properties of bulk and 1D materials.[252] Similarly, the electronic properties of 2D piezoelectric materials are also affected by the applied strain, owing to the fact that piezoelectric charges possibly affect the related quantum yield; hence understanding the influence of strain on 2D piezoelectric materials can expand their further applications. Dielectricity is another important factor which affects the electromechanical performance of piezoelectric materials; however, to date, only a few reports have addressed this.[10]

Pyroelectricity is another attractive concept that was proposed in some 2D piezoelectric nanostructures, and is assumed as a promising research field for designing new devices. Similarly, 2D ferroelectric materials present some advantages (such as flexibility and band gap tunability) over the conventional bulk ferroelectrics; however, research on the ferroelectricity in 2D materials is in its initial and tentative stage. Therefore, the research field of 2D materials can be promoted by further research on the different aspects of ferroelectricity and pyroelectricity in 2D materials. Diverse 2D piezoelectric materials such as TMDC nanosheets are also biocompatible, leading to exciting prospects for real-world applications and research translation in biotechnology.[213] These 2D piezoelectric materials can be functionalized or covered by biocompatible polymers such as polyethylene glycol (PEG) to guarantee a long-term combinatorial therapy. They can be actuated *via* electric fields to release drugs and target diseased cells. Additionally, lead-based piezoelectric materials can be replaced by biocompatible 2D materials in self-powered piezoelectric implantable devices to avoid replacing discharged batteries and further invasive operation.

Conflicts of interest

The authors have no conflicts of interest to declare.

Acknowledgements

The authors gratefully acknowledge the Australian Research Council (ARC) Centre of Excellence FLEET (CE170100039) for the financial support in this work.

References

1 H. Liu, J. Zhong, C. Lee, S.-W. Lee and L. Lin, *Appl. Phys. Rev.*, 2018, **5**, 1–35.
2 R. Hinchet, U. Khan, C. Falconi and S.-W. Kim, *Mater. Today*, 2018, **21**, 611–630.
3 Z. Fei, W. Zhao, T. A. Palomaki, B. Sun, M. K. Miller, Z. Zhao, J. Yan, X. Xu and D. H. Cobden, *Nature*, 2018, **560**, 336–339.
4 X. Q. Fang, J. X. Liu and V. Gupta, *Nanoscale*, 2013, **5**, 1716–1726.
5 J. N. Tiwari, R. N. Tiwari and K. S. Kim, *Prog. Mater. Sci.*, 2012, **57**, 724–803.
6 L. Liang, X. Kang, Y. Sang and H. Liu, *Adv. Sci.*, 2016, **3**, 1500358.
7 J. Varghese, R. W. Whatmore and J. D. Holmes, *J. Mater. Chem. C*, 2013, **1**, 2618–2638.
8 H. D. Espinosa, R. A. Bernal and M. Minary-Jolandan, *Adv. Mater.*, 2012, **24**, 4656–4675.
9 M. B. Ghasemian, A. Rawal, F. Wang, D. Chu and D. Wang, *J. Mater. Chem. C*, 2017, **5**, 10976–10984.
10 J. Zhang, C. Wang and C. Bowen, *Nanoscale*, 2014, **6**, 13314–13327.
11 W. Wu, C. Pan, Y. Zhang, X. Wen and Z. L. Wang, *Nano Today*, 2013, **8**, 619–642.
12 K. Gupta, S. Brahma, J. Dutta, B. Rao and C.-P. Liu, *Nano Energy*, 2019, **55**, 1–21.
13 K. S. Novoselov, D. Jiang, F. Schedin, T. J. Booth, V. V. Khotkevich, S. V. Morozov and A. K. Geim, *Proc. Natl. Acad. Sci. U. S. A.*, 2005, **102**, 10451.
14 W. Wu, L. Wang, Y. Li, F. Zhang, L. Lin, S. Niu, D. Chenet, X. Zhang, Y. Hao, T. F. Heinz, J. Hone and Z. L. Wang, *Nature*, 2014, **514**, 470–474.
15 P. Lin, C. Pan and Z. L. Wang, *Mater. Today Nano*, 2018, **4**, 17–31.
16 L. Newton, T. Slater, N. Clark and A. Vijayaraghavan, *J. Mater. Chem. C*, 2013, **1**, 376–393.
17 T. Wu and H. Zhang, *Angew. Chem., Int. Ed.*, 2015, **54**, 4432–4434.
18 X. Zhang, A. Chen and Z. Zhou, *Wiley Interdiscip. Rev.: Comput. Mol. Sci.*, 2019, **9**, 1–15.
19 H. Tian, J. Tice, R. Fei, V. Tran, X. Yan, L. Yang and H. Wang, *Nano Today*, 2016, **11**, 763–777.
20 Q. H. Wang, K. Kalantar-Zadeh, A. Kis, J. N. Coleman and M. S. Strano, *Nat. Nanotechnol.*, 2012, **7**, 699–712.
21 S. Balendhran, J. Deng, J. Z. Ou, S. Walia, J. Scott, J. Tang, K. L. Wang, M. R. Field, S. Russo, S. Zhuiykov, M. S. Strano, N. Medhekar, S. Sriram, M. Bhaskaran and K. Kalantar-zadeh, *Adv. Mater.*, 2013, **25**, 109–114.
22 A. Molina-Sanchez and L. Wirtz, *Phys. Rev. B: Condens. Matter Mater. Phys.*, 2011, **84**, 155413.
23 Y. Li, Y. Rao, K. F. Mak, Y. You, S. Wang, C. R. Dean and T. F. Heinz, *Nano Lett.*, 2013, **13**, 3329–3333.
24 J. Zhao, N. Li, H. Yu, Z. Wei, M. Liao, P. Chen, S. Wang, D. Shi, Q. Sun and G. Zhang, *Adv. Mater.*, 2017, **29**, 1702076.
25 M. Yagmurcukardes, C. Bacaksiz, E. Unsal, B. Akbali, R. T. Senger and H. Sahin, *Phys. Rev. B: Condens. Matter Mater. Phys.*, 2018, **97**, 115427.
26 H. Zhan, D. Guo and G. Xie, *Nanoscale*, 2019, **11**, 13181–13212.
27 R. Li, Y. Cheng and W. Huang, *Small*, 2018, **14**, 1802091.
28 Y. Liu, E. T. N. Wahyudin, J.-H. He and J. Zhai, *MRS Bull.*, 2018, **43**, 959–964.

29 K.-A. N. Duerloo, M. T. Ong and E. J. Reed, *J. Phys. Chem. Lett.*, 2012, **3**, 2871–2876.
30 E. K. Akdogan, M. Allahverdi and A. Safari, *IEEE Trans. Ultrason. Ferroelectr. Freq. Control*, 2005, **52**, 746–775.
31 F. R. Fan, W. Tang and Z. L. Wang, *Adv. Mater.*, 2016, **28**, 4283–4305.
32 Z. L. Wang, *Nano Today*, 2010, **5**, 540–552.
33 C. R. Bowen, H. A. Kim, P. M. Weaver and S. Dunn, *Chem. Rev.*, 2014, **7**, 25–44.
34 E. Aksel and J. L. Jones, *Sensors*, 2010, **10**, 1935–1954.
35 P. Miro, M. Audiffred and T. Heine, *Chem. Soc. Rev.*, 2014, **43**, 6537–6554.
36 C. Cui, F. Xue, W.-J. Hu and L.-J. Li, *npj 2D Mater. Appl.*, 2018, **2**, 1–14.
37 M. N. Blonsky, H. L. Zhuang, A. K. Singh and R. G. Hennig, *ACS Nano*, 2015, **9**, 9885–9891.
38 Z. C. Tu and X. Hu, *Phys. Rev. B: Condens. Matter Mater. Phys.*, 2006, **74**, 035434.
39 M. T. Ong and E. J. Reed, *ACS Nano*, 2012, **6**, 1387–1394.
40 M. M. Alyoruk, Y. Aierken, D. Cakir, F. M. Peeters and C. Sevik, *J. Phys. Chem. C*, 2015, **119**, 23231–23237.
41 W. Li and J. Li, *Nano Res.*, 2015, **8**, 3796–3802.
42 R. Fei, W. Li, J. Li and L. Yang, *Appl. Phys. Lett.*, 2015, **107**, 173104.
43 J. Zhang and S. A. Meguid, *Semicond. Sci. Technol.*, 2017, **32**, 1–20.
44 F. Xue, J. Zhang, W. Hu, W.-T. Hsu, A. Han, S.-F. Leung, J.-K. Huang, Y. Wan, S. Liu, J. Zhang, J.-H. He, W.-H. Chang, Z. L. Wang, X. Zhang and L.-J. Li, *ACS Nano*, 2018, **12**, 4976–4983.
45 F. Xue, X. He, J. R. D. Retamal, A. Han, J. Zhang, Z. Liu, J.-K. Huang, W. Hu, V. Tung, J.-H. He, L.-J. Li and X. Zhang, *Adv. Mater.*, 2019, **31**, 1901300.
46 Y.-L. Su, K. Gupta, Y.-L. Hsiao, R.-C. Wang and C.-P. Liu, *Energy Environ. Sci.*, 2019, **12**, 410–417.
47 J. F. Nye, *Physical properties of crystals: their representation by tensors and matrices*, Clarendon, Oxford, 1957.
48 G. Cheon, K. N. Duerloo, A. D. Sendek, C. Porter, Y. Chen and E. J. Reed, *Nano Lett.*, 2017, **17**, 1915–1923.
49 H. L. Zhuang, A. K. Singh and R. G. Hennig, *Phys. Rev. B: Condens. Matter Mater. Phys.*, 2013, **87**, 1–8.
50 H. L. Zhuang and R. G. Hennig, *J. Phys. Chem. C*, 2013, **117**, 20440–20445.
51 H. Zhu, Y. Wang, J. Xiao, M. Liu, S. Xiong, Z. J. Wong, Z. Ye, Y. Ye, X. Yin and X. Zhang, *Nat. Nanotechnol.*, 2015, **10**, 151–155.
52 F. Wang, J. H. Seo, G. Luo, M. B. Starr, Z. Li, D. Geng, X. Yin, S. Wang, D. G. Fraser, D. Morgan, Z. Ma and X. Wang, *Nat. Commun.*, 2016, **7**, 10444.
53 L. Wang, S. Liu, G. Gao, Y. Pang, X. Yin, X. Feng, L. Zhu, Y. Bai, L. Chen, T. Xiao, X. Wang, Y. Qin and Z. L. Wang, *ACS Nano*, 2018, **12**, 4903–4908.
54 X. Wang, X. He, H. Zhu, L. Sun, W. Fu, X. Wang, L. C. Hoong, H. Wang, Q. Zeng, W. Zhao, J. Wei, Z. Jin, Z. Shen, J. Liu, T. Zhang and Z. Liu, *Sci. Adv.*, 2016, **2**, 1600209.
55 R. Agrawal and H. D. Espinosa, *Nano Lett.*, 2011, **11**, 786–790.
56 C.-H. Wang, W.-S. Liao, Z.-H. Lin, N.-J. Ku, Y.-C. Li, Y.-C. Chen, Z.-L. Wang and C.-P. Liu, *Adv. Energy Mater.*, 2014, **4**, 1400392.
57 T. Ogawa, H. Oikawa and A. Kojima, *Jpn. J. Appl. Phys.*, 1971, **10**, 593–599.
58 D. A. Scrymgeour and J. W. Hsu, *Nano Lett.*, 2008, **8**, 2204–2209.
59 L. Wang, S. Liu, Z. Zhang, X. Feng, L. Zhu, H. Guo, W. Ding, L. Chen, Y. Qin and Z. L. Wang, *Nano Energy*, 2019, **60**, 724–733.
60 M. T. Ong, K.-A. N. Duerloo and E. J. Reed, *J. Phys. Chem. C*, 2013, **117**, 3615–3620.
61 E. W. Hill, A. Vijayaragahvan and K. Novoselov, *IEEE Sens. J.*, 2011, **11**, 3161–3170.
62 G. da Cunha Rodrigues, P. Zelenovskiy, K. Romanyuk, S. Luchkin, Y. Kopelevich and A. Kholkin, *Nat. Commun.*, 2015, **6**, 7572.
63 K. E. El-Kelany, P. Carbonniere, A. Erba and M. Rerat, *J. Phys. Chem. C*, 2015, **119**, 8966–8973.
64 M. Zelisko, Y. Hanlumyuang, S. Yang, Y. Liu, C. Lei, J. Li, P. M. Ajayan and P. Sharma, *Nat. Commun.*, 2014, **5**, 4284.
65 B. Javvaji, B. He and X. Zhuang, *Nanotechnology*, 2018, **29**, 225702.
66 S. Chandratre and P. Sharma, *Appl. Phys. Lett.*, 2012, **100**, 1–3.
67 O. Leenaerts, H. Peelaers, A. D. Hernandez-Nieves, B. Partoens and F. M. Peeters, *Phys. Rev. B: Condens. Matter Mater. Phys.*, 2010, **82**, 195436.
68 P. V. Medeiros, A. J. Mascarenhas, F. de Brito Mota and C. M. de Castilho, *Nanotechnology*, 2010, **21**, 485701.
69 K.-H. Jin, S.-M. Choi and S.-H. Jhi, *Phys. Rev. B: Condens. Matter Mater. Phys.*, 2010, **82**, 033414.
70 D. W. Boukhvalov and M. I. Katsnelson, *J. Phys.: Condens. Matter*, 2009, **21**, 344205.
71 J. H. Chen, C. Jang, S. Adam, M. S. Fuhrer, E. D. Williams and M. Ishigami, *Nat. Phys.*, 2008, **4**, 377–381.
72 X. Wang, G. Sun, P. Routh, D. H. Kim, W. Huang and P. Chen, *Chem. Soc. Rev.*, 2014, **43**, 7067–7098.
73 B. Li, L. Zhou, D. Wu, H. Peng, K. Yan, Y. Zhou and Z. Liu, *ACS Nano*, 2011, **5**, 5957–5961.
74 A. A. M. Noor, H. J. Kim and Y. H. Shin, *Phys. Chem. Chem. Phys.*, 2014, **16**, 6575–6582.
75 R. S. Dahiya and M. Valle, *Robotic tactile sensing: technologies and system*, Springer Science & Business Media, 2012.
76 K. Shimada, *Jpn. J. Appl. Phys.*, 2006, **45**, 358–360.
77 A. Hangleiter, F. Hitzel, S. Lahmann and U. Rossow, *Appl. Phys. Lett.*, 2003, **83**, 1169–1171.
78 S. Trolier-McKinstry and P. Muralt, *J. Electroceram.*, 2004, **12**, 7–17.
79 M. Kratzer, M. Lasnik, S. Rohrig, C. Teichert and M. Deluca, *Sci. Rep.*, 2018, **8**, 422.
80 S. R. Moheimani and A. J. Fleming, *Piezoelectric transducers for vibration control and damping*, Springer Science & Business Media, 2006.

81 A. Safari and E. K. Akdogan, *Piezoelectric and acoustic materials for transducer applications*, Springer US, 2008.
82 Y. Zhou, D. Wu, Y. Zhu, Y. Cho, Q. He, X. Yang, K. Herrera, Z. Chu, Y. Han, M. C. Downer, H. Peng and K. Lai, *Nano Lett.*, 2017, **17**, 5508–5513.
83 C. Cui, W. J. Hu, X. Yan, C. Addiego, W. Gao, Y. Wang, Z. Wang, L. Li, Y. Cheng, P. Li, X. Zhang, H. N. Alshareef, T. Wu, W. Zhu, X. Pan and L. J. Li, *Nano Lett.*, 2018, **18**, 1253–1258.
84 A.-Y. Lu, H. Zhu, J. Xiao, C.-P. Chuu, Y. Han, M.-H. Chiu, C.-C. Cheng, C.-W. Yang, K.-H. Wei, Y. Yang, Y. Wang, D. Sokaras, D. Nordlund, P. Yang, D. A. Muller, M.-Y. Chou, X. Zhang and L.-J. Li, *Nat. Nanotechnol.*, 2017, **12**, 744.
85 N. Mahmood, I. A. De Castro, K. Pramoda, K. Khoshmanesh, S. K. Bhargava and K. Kalantar-Zadeh, *Energy Storage Mater.*, 2019, **16**, 455–480.
86 T. Zhang, J. Liu, C. Wang, X. Leng, Y. Xiao and L. Fu, *Biosens. Bioelectron.*, 2017, **89**, 28–42.
87 K. Kalantar-zadeh, A. Vijayaraghavan, M.-H. Ham, H. Zheng, M. Breedon and M. S. Strano, *Chem. Mater.*, 2010, **22**, 5660–5666.
88 V. Nicolosi, M. Chhowalla, M. G. Kanatzidis, M. S. Strano and J. N. Coleman, *Science*, 2013, **340**, 1226419.
89 X. Huang, Z. Zeng and H. Zhang, *Chem. Soc. Rev.*, 2013, **42**, 1934–1946.
90 J. Z. Ou, A. F. Chrimes, Y. Wang, S. Y. Tang, M. S. Strano and K. Kalantar-zadeh, *Nano Lett.*, 2014, **14**, 857–863.
91 M. G. Donato, E. Messina, A. Foti, T. J. Smart, P. H. Jones, M. A. Iati, R. Saija, P. G. Gucciardi and O. M. Marago, *Nanoscale*, 2018, **10**, 1245–1255.
92 J. N. Coleman, M. Lotya, A. O'Neill, S. D. Bergin, P. J. King, U. Khan, K. Young, A. Gaucher, S. De, R. J. Smith, I. V. Shvets, S. K. Arora, G. Stanton, H. Y. Kim, K. Lee, G. T. Kim, G. S. Duesberg, T. Hallam, J. J. Boland, J. J. Wang, J. F. Donegan, J. C. Grunlan, G. Moriarty, A. Shmeliov, R. J. Nicholls, J. M. Perkins, E. M. Grieveson, K. Theuwissen, D. W. McComb, P. D. Nellist and V. Nicolosi, *Science*, 2011, **331**, 568–571.
93 L. Li, Y. Yu, G. J. Ye, Q. Ge, X. Ou, H. Wu, D. Feng, X. H. Chen and Y. Zhang, *Nat. Nanotechnol.*, 2014, **9**, 372–377.
94 M. Naguib, V. N. Mochalin, M. W. Barsoum and Y. Gogotsi, *Adv. Mater.*, 2014, **26**, 992–1005.
95 R. J. Smith, P. J. King, M. Lotya, C. Wirtz, U. Khan, S. De, A. O'Neill, G. S. Duesberg, J. C. Grunlan, G. Moriarty, J. Chen, J. Wang, A. I. Minett, V. Nicolosi and J. N. Coleman, *Adv. Mater.*, 2011, **23**, 3944–3948.
96 K. Choudhary, I. Kalish, R. Beams and F. Tavazza, *Sci. Rep.*, 2017, **7**, 5179.
97 T. Björkman, A. Gulans, A. V. Krasheninnikov and R. M. Nieminen, *Phys. Rev. Lett.*, 2012, **108**, 235502.
98 M. Ashton, J. Paul, S. B. Sinnott and R. G. Hennig, *Phys. Rev. Lett.*, 2017, **118**, 106101.
99 N. Mounet, M. Gibertini, P. Schwaller, D. Campi, A. Merkys, A. Marrazzo, T. Sohier, I. E. Castelli, A. Cepellotti, G. Pizzi and N. Marzari, *Nat. Nanotechnol.*, 2018, **13**, 246–252.
100 S. L. Wong, H. Liu and D. Chi, *Prog. Cryst. Growth Charact. Mater.*, 2016, **62**, 9–28.
101 W. Feng, W. Zheng, F. Gao, X. Chen, G. Liu, T. Hasan, W. Cao and P. Hu, *Chem. Mater.*, 2016, **28**, 4278–4283.
102 J. Qi, Y. W. Lan, A. Z. Stieg, J. H. Chen, Y. L. Zhong, L. J. Li, C. D. Chen, Y. Zhang and K. L. Wang, *Nat. Commun.*, 2015, **6**, 7430.
103 Y.-H. Chang, W. Zhang, Y. Zhu, Y. Han, J. Pu, J.-K. Chang, W.-T. Hsu, J.-K. Huang, C.-L. Hsu, M.-H. Chiu, T. Takenobu, H. Li, C.-I. Wu, W.-H. Chang, A. T. S. Wee and L.-J. Li, *ACS Nano*, 2014, **8**, 8582–8590.
104 S. K. Kim, R. Bhatia, T.-H. Kim, D. Seol, J. H. Kim, H. Kim, W. Seung, Y. Kim, Y. H. Lee and S.-W. Kim, *Nano Energy*, 2016, **22**, 483–489.
105 J. Chen, B. Liu, Y. Liu, W. Tang, C. T. Nai, L. Li, J. Zheng, L. Gao, Y. Zheng, H. S. Shin, H. Y. Jeong and K. P. Loh, *Adv. Mater.*, 2015, **27**, 6722–6727.
106 Y.-H. Lee, X.-Q. Zhang, W. Zhang, M.-T. Chang, C.-T. Lin, K.-D. Chang, Y.-C. Yu, J. T.-W. Wang, C.-S. Chang, L.-J. Li and T.-W. Lin, *Adv. Mater.*, 2012, **24**, 2320–2325.
107 S. Balendhran, J. Z. Ou, M. Bhaskaran, S. Sriram, S. Ippolito, Z. Vasic, E. Kats, S. Bhargava, S. Zhuiykov and K. Kalantar-zadeh, *Nanoscale*, 2012, **4**, 461–466.
108 K. K. Liu, W. Zhang, Y. H. Lee, Y. C. Lin, M. T. Chang, C. Y. Su, C. S. Chang, H. Li, Y. Shi, H. Zhang, C. S. Lai and L. J. Li, *Nano Lett.*, 2012, **12**, 1538–1544.
109 J. Chen, W. Tang, B. Tian, B. Liu, X. Zhao, Y. Liu, T. Ren, W. Liu, D. Geng, H. Y. Jeong, H. S. Shin, W. Zhou and K. P. Loh, *Adv. Sci.*, 2016, **3**, 1500033.
110 A. M. van der Zande, P. Y. Huang, D. A. Chenet, T. C. Berkelbach, Y. You, G. H. Lee, T. F. Heinz, D. R. Reichman, D. A. Muller and J. C. Hone, *Nat. Mater.*, 2013, **12**, 554–561.
111 M. M. Y. A. Alsaif, N. Pillai, S. Kuriakose, S. Walia, A. Jannat, K. Xu, T. Alkathiri, M. Mohiuddin, T. Daeneke, K. Kalantar-Zadeh, J. Z. Ou and A. Zavabeti, *ACS Appl. Nano Mater.*, 2019, **2**, 4665–4672.
112 B. J. Carey, J. Z. Ou, R. M. Clark, K. J. Berean, A. Zavabeti, A. S. Chesman, S. P. Russo, D. W. Lau, Z. Q. Xu, Q. Bao, O. Kevehei, B. C. Gibson, M. D. Dickey, R. B. Kaner, T. Daeneke and K. Kalantar-Zadeh, *Nat. Commun.*, 2017, **8**, 14482.
113 T. Daeneke, P. Atkin, R. Orrell-Trigg, A. Zavabeti, T. Ahmed, S. Walia, M. Liu, Y. Tachibana, M. Javaid, A. D. Greentree, S. P. Russo, R. B. Kaner and K. Kalantar-Zadeh, *ACS Nano*, 2017, **11**, 10974–10983.
114 A. Zavabeti, B. Y. Zhang, I. A. de Castro, J. Z. Ou, B. J. Carey, M. Mohiuddin, R. Datta, C. Xu, A. P. Mouritz, C. F. McConville, A. P. O'Mullane, T. Daeneke and K. Kalantar-Zadeh, *Adv. Funct. Mater.*, 2018, **28**, 1–9.
115 T. Daeneke, K. Khoshmanesh, N. Mahmood, I. A. de Castro, D. Esrafilzadeh, S. J. Barrow, M. D. Dickey and K. Kalantar-zadeh, *Chem. Soc. Rev.*, 2018, **47**, 4073–4111.

116 A. Zavabeti, J. Z. Ou, B. J. Carey, N. Syed, R. Orrell-Trigg, E. L. H. Mayes, C. Xu, O. Kavehei, A. P. O'Mullane, R. B. Kaner, K. Kalantar-zadeh and T. Daeneke, *Science*, 2017, **358**, 332–335.
117 K. S. Novoselov, A. K. Geim, S. V. Morozov, D. Jiang, Y. Zhang, S. V. Dubonos, I. V. Grigorieva and A. A. Firsov, *Science*, 2004, **306**, 666.
118 N. Syed, A. Zavabeti, J. Z. Ou, M. Mohiuddin, N. Pillai, B. J. Carey, B. Y. Zhang, R. S. Datta, A. Jannat, F. Haque, K. A. Messalea, C. Xu, S. P. Russo, C. F. McConville, T. Daeneke and K. Kalantar-Zadeh, *Nat. Commun.*, 2018, **9**, 3618.
119 Y. Zhang, T. R. Chang, B. Zhou, Y. T. Cui, H. Yan, Z. Liu, F. Schmitt, J. Lee, R. Moore, Y. Chen, H. Lin, H. T. Jeng, S. K. Mo, Z. Hussain, A. Bansil and Z. X. Shen, *Nat. Nanotechnol.*, 2014, **9**, 111–115.
120 Z. Yang, W. Jie, C. H. Mak, S. Lin, H. Lin, X. Yang, F. Yan, S. P. Lau and J. Hao, *ACS Nano*, 2017, **11**, 4225–4236.
121 Z. Yang and J. Hao, *J. Mater. Chem. C*, 2016, **4**, 8859–8878.
122 L. Jiao, W. Jie, Z. Yang, Y. Wang, Z. Chen, X. Zhang, W. Tang, Z. Wu and J. Hao, *J. Mater. Chem. C*, 2019, **7**, 2522–2529.
123 W. Jie, Z. Yang, F. Zhang, G. Bai, C. W. Leung and J. Hao, *ACS Nano*, 2017, **11**, 6950–6958.
124 M. I. Serna, S. H. Yoo, S. Moreno, Y. Xi, J. P. Oviedo, H. Choi, H. N. Alshareef, M. J. Kim, M. Minary-Jolandan and M. A. Quevedo-Lopez, *ACS Nano*, 2016, **10**, 6054–6061.
125 G. Bai, Z. Yang, H. Lin, W. Jie and J. Hao, *Nanoscale*, 2018, **10**, 9261–9267.
126 M. Mohiuddin, Y. Wang, A. Zavabeti, N. Syed, R. S. Datta, H. Ahmed, T. Daeneke, S. P. Russo, A. R. Rezk, L. Y. Yeo and K. Kalantar-Zadeh, *Chem. Mater.*, 2018, **30**, 5593–5601.
127 E. Varrla, C. Backes, K. R. Paton, A. Harvey, Z. Gholamvand, J. McCauley and J. N. Coleman, *Chem. Mater.*, 2015, **27**, 1129–1139.
128 H. Ahmed, A. R. Rezk, B. J. Carey, Y. Wang, M. Mohiuddin, K. J. Berean, S. P. Russo, K. Kalantar-zadeh and L. Y. Yeo, *Adv. Mater.*, 2018, **30**, 1704756.
129 X. Zhuang, B. He, B. Javvaji and H. S. Park, *Phys. Rev. B: Condens. Matter Mater. Phys.*, 2019, **99**, 054105.
130 K. H. Michel and B. Verberck, *Phys. Rev. B: Condens. Matter Mater. Phys.*, 2009, **80**, 1–10.
131 L. C. Gomes, A. Carvalho and A. H. Castro Neto, *Phys. Rev. B: Condens. Matter Mater. Phys.*, 2015, **92**, 1–8.
132 A. K. Singh, K. Mathew, H. L. Zhuang and R. G. Hennig, *J. Phys. Chem. Lett.*, 2015, **6**, 1087–1098.
133 H. Wei, H. Wang, Y. Xia, D. Cui, Y. Shi, M. Dong, C. Liu, T. Ding, J. Zhang, Y. Ma, N. Wang, Z. Wang, Y. Sun, R. Wei and Z. Guo, *J. Mater. Chem. C*, 2018, **6**, 12446–12467.
134 W. Wu and Z. L. Wang, *Nat. Rev. Mater.*, 2016, **1**, 1–17.
135 Y. Zhang, W. Jie, P. Chen, W. Liu and J. Hao, *Adv. Mater.*, 2018, **30**, 1707007.
136 Y. Shi, H. Li and L. J. Li, *Chem. Soc. Rev.*, 2015, **44**, 2744–2756.
137 J. E. ten Elshof, H. Yuan and P. Gonzalez Rodriguez, *Adv. Energy Mater.*, 2016, **6**, 1–34.
138 M. Chhowalla, H. S. Shin, G. Eda, L. J. Li, K. P. Loh and H. Zhang, *Nat. Chem.*, 2013, **5**, 263–275.
139 S. Manzeli, D. Ovchinnikov, D. Pasquier, O. V. Yazyev and A. Kis, *Nat. Rev. Mater.*, 2017, **2**, 1–15.
140 A. Jain, S. P. Ong, G. Hautier, W. Chen, W. D. Richards, S. Dacek, S. Cholia, D. Gunter, D. Skinner, G. Ceder and K. A. Persson, *APL Mater.*, 2013, **1**, 011002.
141 R. Armiento, B. Kozinsky, M. Fornari and G. Ceder, *Phys. Rev. B: Condens. Matter Mater. Phys.*, 2011, **84**, 1–13.
142 W. Liu, A. Zhang, Y. Zhang and Z. L. Wang, *Appl. Phys. Lett.*, 2015, **107**, 1–5.
143 H. L. Zhuang, M. D. Johannes, M. N. Blonsky and R. G. Hennig, *Appl. Phys. Lett.*, 2014, **104**, 1–5.
144 Z. Chang, W. Yan, J. Shang and J. Z. Liu, *Appl. Phys. Lett.*, 2014, **105**, 1–5.
145 A. Kuhn, A. Chevy and R. Chevalier, *Phys. Status Solidi A*, 1975, **31**, 469–475.
146 A. Kuhn, A. Chevy and R. Chevalier, *Acta Crystallogr., Sect. B: Struct. Crystallogr. Cryst. Chem.*, 1976, **32**, 983–984.
147 J. Rigoult, A. Rimsky and A. Kuhn, *Acta Crystallogr., Sect. B: Struct. Crystallogr. Cryst. Chem.*, 1980, **36**, 916–918.
148 O. Madelung, *Semiconductors: Data Handbook*, Springer-Verlag Berlin Heidelberg, 2004.
149 M. Mosaferi, I. Abdolhosseini Sarsari and M. Alaei, *Journal*, 2018, 1–8.
150 M. Mehboudi, B. M. Fregoso, Y. Yang, W. Zhu, A. van der Zande, J. Ferrer, L. Bellaiche, P. Kumar and S. Barraza-Lopez, *Phys. Rev. Lett.*, 2016, **117**, 246802.
151 J. Zhang, *Nano Energy*, 2019, **58**, 568–578.
152 H. S. Song, S. L. Li, L. Gao, Y. Xu, K. Ueno, J. Tang, Y. B. Cheng and K. Tsukagoshi, *Nanoscale*, 2013, **5**, 9666–9670.
153 G. Kim, A. R. Jang, H. Y. Jeong, Z. Lee, D. J. Kang and H. S. Shin, *Nano Lett.*, 2013, **13**, 1834–1839.
154 W. Wang, P. Li, F. Jin and J. Wang, *Compos. Struct.*, 2016, **140**, 758–775.
155 B. J. Alder and T. E. Wainwright, *J. Chem. Phys.*, 1959, **31**, 459–466.
156 D. C. Rapaport, *The Art of Molecular Dynamics Simulation*, Cambridge University Press, 2004.
157 V. Yamakov, C. Park, J. H. Kang, K. E. Wise and C. Fay, *Comput. Mater. Sci.*, 2014, **95**, 362–370.
158 J. Wang, A. J. Kulkarni, K. Sarasamak, S. Limpijumnong, F. J. Ke and M. Zhou, *Phys. Rev. B: Condens. Matter Mater. Phys.*, 2007, **76**, 1–4.
159 K. Momeni, G. M. Odegard and R. S. Yassar, *Acta Mater.*, 2012, **60**, 5117–5124.
160 M. Graf, M. Sepliarsky, R. Machado and M. G. Stachiotti, *Solid State Commun.*, 2015, **218**, 10–13.
161 H. K. Ravi, F. Simona, J. Hulliger and M. Cascella, *J. Phys. Chem. B*, 2012, **116**, 1901–1907.
162 F. Ahmadpoor and P. Sharma, *Nanoscale*, 2015, **7**, 16555–16570.

163 C. Li and T.-W. Chou, *Int. J. Solids Struct.*, 2003, **40**, 2487–2499.
164 K. I. Tserpes and P. Papanikos, *Composites, Part B*, 2005, **36**, 468–477.
165 A. Sakhaee-Pour, M. T. Ahmadian and R. Naghdabadi, *Nanotechnology*, 2008, **19**, 085702.
166 F. Scarpa, S. Adhikari and A. Srikantha Phani, *Nanotechnology*, 2009, **20**, 065709.
167 J. Zhang, C. Wang and S. Adhikari, *J. Phys. D: Appl. Phys.*, 2013, **46**, 1–5.
168 R. Herdier, D. Jenkins, E. Dogheche, D. Remiens and M. Sulc, *Rev. Sci. Instrum.*, 2006, **77**, 1–5.
169 A. R. Rezk, B. Carey, A. F. Chrimes, D. W. Lau, B. C. Gibson, C. Zheng, M. S. Fuhrer, L. Y. Yeo and K. Kalantar-Zadeh, *Nano Lett.*, 2016, **16**, 849–855.
170 C. M. Lueng, H. L. W. Chan, C. Surya, W. K. Fong, C. L. Choy, P. Chow and M. Rosamond, *J. Non-Cryst. Solids*, 1999, **254**, 123–127.
171 F. Xu, F. Chu and S. Trolier-McKinstry, *J. Appl. Phys.*, 1999, **86**, 588–594.
172 H. Ohigashi, *J. Appl. Phys.*, 1976, **47**, 949–955.
173 T. Takenaka, K. O. Sakata and K. O. Toda, *Ferroelectrics*, 1990, **106**, 375–380.
174 L. Zhu, P. Lin, B. Chen, L. Wang, L. Chen, D. Li and Z. L. Wang, *Nano Res.*, 2018, **11**, 3877–3885.
175 S. V. Kalinin, A. Rar and S. Jesse, *IEEE Trans. Ultrason. Ferroelectr. Freq. Control*, 2006, **53**, 2226–2252.
176 S. V. Kalinin and A. Gruverman, *Scanning probe microscopy: electrical and electromechanical phenomena at the nanoscale*, Springer, New York, 2007.
177 M.-H. Zhang, H. C. Thong, Y. X. Lu, W. Sun, J.-F. Li and K. Wang, *J. Korean Ceram. Soc.*, 2017, **54**, 261–271.
178 E. Soergel, *J. Phys. D: Appl. Phys.*, 2011, **44**, 1–17.
179 H. Miao, X. Zhou, S. Dong, H. Luo and F. Li, *Nanoscale*, 2014, **6**, 8515–8520.
180 J. Seidel, L. W. Martin, Q. He, Q. Zhan, Y. H. Chu, A. Rother, M. E. Hawkridge, P. Maksymovych, P. Yu, M. Gajek, N. Balke, S. V. Kalinin, S. Gemming, F. Wang, G. Catalan, J. F. Scott, N. A. Spaldin, J. Orenstein and R. Ramesh, *Nat. Mater.*, 2009, **8**, 229–234.
181 S. V. Kalinin, S. Jesse, B. J. Rodriguez, J. Shin, A. P. Baddorf, H. N. Lee, A. Borisevich and S. J. Pennycook, *Nanotechnology*, 2006, **17**, 3400–3411.
182 L. You, Z. Chen, X. Zou, H. Ding, W. Chen, L. Chen, G. Yuan and J. Wang, *ACS Nano*, 2012, **6**, 5388–5394.
183 S. J. Rothberg, M. S. Allen, P. Castellini, D. Di Maio, J. J. J. Dirckx, D. J. Ewins, B. J. Halkon, P. Muyshondt, N. Paone, T. Ryan, H. Steger, E. P. Tomasini, S. Vanlanduit and J. F. Vignola, *Opt. Lasers Eng.*, 2017, **99**, 11–22.
184 Z. Wang and J. Miao, *J. Phys. D: Appl. Phys.*, 2008, **41**, 1–7.
185 J. Hernando, J. L. Sánchez-Rojas, S. González-Castilla, E. Iborra, A. Ababneh and U. Schmid, *J. Appl. Phys.*, 2008, **104**, 053502.
186 V. Edon, D. Remiens and S. Saada, *Appl. Surf. Sci.*, 2009, **256**, 1455–1460.
187 S. Quignon, C. Soyer and D. Remiens, *J. Am. Ceram. Soc.*, 2012, **95**, 3180–3184.
188 R. W. Boyd, in *Nonlinear Optics*, ed. R. W. Boyd, Academic Press, Burlington, 3rd edn, 2008, pp. 1–67.
189 S. A. Denev, T. T. A. Lummen, E. Barnes, A. Kumar, V. Gopalan and D. J. Green, *J. Am. Ceram. Soc.*, 2011, **94**, 2699–2727.
190 L. M. Malard, T. V. Alencar, A. P. M. Barboza, K. F. Mak and A. M. de Paula, *Phys. Rev. B: Condens. Matter Mater. Phys.*, 2013, **87**, 1–5.
191 H. Yokota, R. Haumont, J.-M. Kiat, H. Matsuura and Y. Uesu, *Appl. Phys. Lett.*, 2009, **95**, 1–3.
192 N. Kumar, S. Najmaei, Q. Cui, F. Ceballos, P. M. Ajayan, J. Lou and H. Zhao, *Phys. Rev. B: Condens. Matter Mater. Phys.*, 2013, **87**, 1–6.
193 F. Liu, L. You, K. L. Seyler, X. Li, P. Yu, J. Lin, X. Wang, J. Zhou, H. Wang, H. He, S. T. Pantelides, W. Zhou, P. Sharma, X. Xu, P. M. Ajayan, J. Wang and Z. Liu, *Nat. Commun.*, 2016, **7**, 12357.
194 H. Li, Y. Shi, M.-H. Chiu and L.-J. Li, *Nano Energy*, 2015, **18**, 293–305.
195 H.-J. Jin, W. Y. Yoon and W. Jo, *ACS Appl. Mater. Interfaces*, 2018, **10**, 1334–1339.
196 W. Liu, Y. Zhou, A. Zhang, Y. Zhang and Z. L. Wang, *Appl. Phys. Lett.*, 2016, **108**, 1–5.
197 Y. Zhou, W. Liu, X. Huang, A. Zhang, Y. Zhang and Z. L. Wang, *Nano Res.*, 2016, **9**, 800–807.
198 M. López-Suárez, M. Pruneda, G. Abadal and R. Rurali, *Nanotechnology*, 2014, **25**, 175401.
199 H. Wang, H. Feng and J. Li, *Small*, 2014, **10**, 2165–2181.
200 D. Chen, G. Ji, B. Ding, Y. Ma, B. Qu, W. Chen and J. Y. Lee, *Nanoscale*, 2013, **5**, 7890–7896.
201 C.-J. Liu, S.-Y. Tai, S.-W. Chou, Y.-C. Yu, K.-D. Chang, S. Wang, F. S.-S. Chien, J.-Y. Lin and T.-W. Lin, *J. Mater. Chem.*, 2012, **22**, 21057–21064.
202 Y. Qi, Q. Xu, Y. Wang, B. Yan, Y. Ren and Z. Chen, *ACS Nano*, 2016, **10**, 2903–2909.
203 Z. Yin, H. Li, H. Li, L. Jiang, Y. Shi, Y. Sun, G. Lu, Q. Zhang, X. Chen and H. Zhang, *ACS Nano*, 2012, **6**, 74–80.
204 B. W. Baugher, H. O. Churchill, Y. Yang and P. Jarillo-Herrero, *Nat. Nanotechnol.*, 2014, **9**, 262–267.
205 A. Dankert, L. Langouche, M. V. Kamalakar and S. P. Dash, *ACS Nano*, 2014, **8**, 476–482.
206 H. Y. Chang, M. N. Yogeesh, R. Ghosh, A. Rai, A. Sanne, S. Yang, N. Lu, S. K. Banerjee and D. Akinwande, *Adv. Mater.*, 2016, **28**, 1818–1823.
207 F. Xue, L. Chen, J. Chen, J. Liu, L. Wang, M. Chen, Y. Pang, X. Yang, G. Gao, J. Zhai and Z. L. Wang, *Adv. Mater.*, 2016, **28**, 3391–3398.
208 W. Wu, L. Wang, R. Yu, Y. Liu, S.-H. Wei, J. Hone and Z. L. Wang, *Adv. Mater.*, 2016, **28**, 8463–8468.
209 J. Martin-Sanchez, R. Trotta, A. Mariscal, R. Serna, G. Piredda, S. Stroj, J. Edlinger, C. Schimpf, J. Aberl, T. Lettner, J. Wildmann, H. Huang, X. Yuan, D. Ziss,

J. Stangl and A. Rastelli, *Semicond. Sci. Technol.*, 2018, **33**, 1–39.
210 J. Z. Ou, W. Ge, B. Carey, T. Daeneke, A. Rotbart, W. Shan, Y. Wang, Z. Fu, A. F. Chrimes, W. Wlodarski, S. P. Russo, Y. X. Li and K. Kalantar-zadeh, *ACS Nano*, 2015, **9**, 10313–10323.
211 K. J. Berean, J. Z. Ou, T. Daeneke, B. J. Carey, E. P. Nguyen, Y. Wang, S. P. Russo, R. B. Kaner and K. Kalantar-Zadeh, *Small*, 2015, **11**, 5035–5040.
212 J. Guo, R. Wen, Y. Liu, K. Zhang, J. Kou, J. Zhai and Z. L. Wang, *ACS Appl. Mater. Interfaces*, 2018, **10**, 8110–8116.
213 V. Agarwal and K. Chatterjee, *Nanoscale*, 2018, **10**, 16365–16397.
214 H. Chen, T. Liu, Z. Su, L. Shang and G. Wei, *Nanoscale Horiz.*, 2018, **3**, 74–89.
215 W. Yin, L. Yan, J. Yu, G. Tian, L. Zhou, X. Zheng, X. Zhang, Y. Yong, J. Li, Z. Gu and Y. Zhao, *ACS Nano*, 2014, **8**, 6922–6933.
216 Z. L. Wang and W. Wu, *Natl. Sci. Rev.*, 2013, **1**, 62–90.
217 W. Hu, C. Zhang and Z. L. Wang, *Nanotechnology*, 2018, **30**, 042001.
218 Z. L. Wang, *Adv. Mater.*, 2012, **24**, 4632–4646.
219 J. Zhou, Y. Gu, P. Fei, W. Mai, Y. Gao, R. Yang, G. Bao and Z. L. Wang, *Nano Lett.*, 2008, **8**, 3035–3040.
220 C.-H. Wang, K.-Y. Lai, Y.-C. Li, Y.-C. Chen and C.-P. Liu, *Adv. Mater.*, 2015, **27**, 6289–6295.
221 J. H. He, C. L. Hsin, J. Liu, L. J. Chen and Z. L. Wang, *Adv. Mater.*, 2007, **19**, 781–784.
222 W. Hu, K. Kalantar-Zadeh, K. Gupta and C.-P. Liu, *MRS Bull.*, 2018, **43**, 936–940.
223 K. Jenkins, V. Nguyen, R. Zhu and R. Yang, *Sensors*, 2015, **15**, 22914–22940.
224 C. Rocke, S. Zimmermann, A. Wixforth, J. P. Kotthaus, G. Böhm and G. Weimann, *Phys. Rev. Lett.*, 1997, **78**, 4099–4102.
225 C. Du, W. Hu and Z. L. Wang, *Adv. Eng. Mater.*, 2018, **20**, 1700760.
226 C. Pan, M. Chen, R. Yu, Q. Yang, Y. Hu, Y. Zhang and Z. L. Wang, *Adv. Mater.*, 2016, **28**, 1535–1552.
227 L. Zhu, P. Lin, B. Chen, L. Wang, L. Chen, D. Li and Z. L. Wang, *Nano Res.*, 2018, **11**, 3877–3885.
228 P. Lin, L. Zhu, D. Li, L. Xu and Z. L. Wang, *Nanoscale*, 2018, **10**, 14472–14479.
229 P. Lin, X. Chen, X. Yan, Z. Zhang, H. Yuan, P. Li, Y. Zhao and Y. Zhang, *Nano Res.*, 2014, **7**, 860–868.
230 C. Jiang, Y. Chen, J. Sun, L. Jing, M. Liu, T. Liu, Y. Pan, X. Pu, B. Ma, W. Hu and Z. L. Wang, *Nano Energy*, 2019, **57**, 300–306.
231 W. Sha, J. Zhang, S. Tan, X. Luo and W. Hu, *J. Phys. D: Appl. Phys.*, 2019, **52**, 213003.
232 Y. Hu, Y. Chang, P. Fei, R. L. Snyder and Z. L. Wang, *ACS Nano*, 2010, **4**, 1234–1240.
233 D. Q. Zheng, Z. Zhao, R. Huang, J. Nie, L. Li and Y. Zhang, *Nano Energy*, 2017, **32**, 448–453.
234 J. H. Lee, J. Y. Park, E. B. Cho, T. Y. Kim, S. A. Han, T. H. Kim, Y. Liu, S. K. Kim, C. J. Roh, H. J. Yoon, H. Ryu, W. Seung, J. S. Lee, J. Lee and S. W. Kim, *Adv. Mater.*, 2017, **29**, 1–7.
235 H. Song, I. Karakurt, M. Wei, N. Liu, Y. Chu, J. Zhong and L. Lin, *Nano Energy*, 2018, **49**, 7–13.
236 F. Ding, H. Ji, Y. Chen, A. Herklotz, K. Dorr, Y. Mei, A. Rastelli and O. G. Schmidt, *Nano Lett.*, 2010, **10**, 3453–3458.
237 S. Liu, L. Wang, X. Feng, Z. Wang, Q. Xu, S. Bai, Y. Qin and Z. L. Wang, *Adv. Mater.*, 2017, **29**, 1606346.
238 Y. Zhang, W. Jie, P. Chen, W. Liu and J. Hao, *Adv. Mater.*, 2018, **30**, 1707007.
239 J. Martin-Sanchez, A. Mariscal, M. De Luca, A. T. Martin-Luengo, G. Gramse, A. Halilovic, R. Serna, A. Bonanni, I. Zardo, R. Trotta and A. Rastelli, *Nano Res.*, 2018, **11**, 1399–1414.
240 Y. Y. Hui, X. Liu, W. Jie, N. Y. Chan, J. Hao, Y.-T. Hsu, L.-J. Li, W. Guo and S. P. Lau, *ACS Nano*, 2013, **7**, 7126–7131.
241 R. Kurapati, K. Kostarelos, M. Prato and A. Bianco, *Adv. Mater.*, 2016, **28**, 6052–6074.
242 K.-H. Kim, B. Kumar, K. Y. Lee, H.-K. Park, J.-H. Lee, H. H. Lee, H. Jun, D. Lee and S.-W. Kim, *Sci. Rep.*, 2013, **3**, 2017.
243 C.-H. Wang, W.-S. Liao, N.-J. Ku, Y.-C. Li, Y.-C. Chen, L.-W. Tu and C.-P. Liu, *Small*, 2014, **10**, 4718–4725.
244 D. H. Kim, H. J. Shin, H. Lee, C. K. Jeong, H. Park, G.-T. Hwang, H.-Y. Lee, D. J. Joe, J. H. Han, S. H. Lee, J. Kim, B. Joung and K. J. Lee, *Adv. Funct. Mater.*, 2017, **27**, 1–8.
245 Q. Zheng, B. Shi, Z. Li and Z. L. Wang, *Adv. Sci.*, 2017, **4**, 1700029.
246 X. Pu, L. Li, M. Liu, C. Jiang, C. Du, Z. Zhao, W. Hu and Z. L. Wang, *Adv. Mater.*, 2016, **28**, 98–105.
247 G. R. Bhimanapati, Z. Lin, V. Meunier, Y. Jung, J. Cha, S. Das, D. Xiao, Y. Son, M. S. Strano, V. R. Cooper, L. Liang, S. G. Louie, E. Ringe, W. Zhou, S. S. Kim, R. R. Naik, B. G. Sumpter, H. Terrones, F. Xia, Y. Wang, J. Zhu, D. Akinwande, N. Alem, J. A. Schuller, R. E. Schaak, M. Terrones and J. A. Robinson, *ACS Nano*, 2015, **9**, 11509–11539.
248 J. Zhang, Y. Chen and X. Wang, *Energy Environ. Sci.*, 2015, **8**, 3092–3108.
249 H. O. H. Churchill and P. Jarillo-Herrero, *Nat. Nanotechnol.*, 2014, **9**, 330.
250 M. E. Davila, L. Xian, S. Cahangirov, A. Rubio and G. Le Lay, *New J. Phys.*, 2014, **16**, 095002.
251 L. Tao, E. Cinquanta, D. Chiappe, C. Grazianetti, M. Fanciulli, M. Dubey, A. Molle and D. Akinwande, *Nat. Nanotechnol.*, 2015, **10**, 227–231.
252 H. Y. S. Al-Zahrani, J. Pal, M. A. Migliorato, G. Tse and D. Yu, *Nano Energy*, 2015, **14**, 382–391.